Atti del

III Convegno Nazionale
Interazioni tra Campi Elettromagnetici e Biosistemi
Napoli 2-4 luglio 2014

ISBN: 9788894008906

con il contributo di

Indice

Effetti Biologici (Sessione 1)

Valutazione Esposizione Elettromagnetica

Applicazioni Medicali (Sessione 1)

Effetti biologici (Sessione 2)

Effetti Biologici (Sessione 2)

MRI

Valutazione del rischio ed implicazioni legali

Sessione di chiusura

Improved protection against methylglyoxal and re-programming of energy metabolism as novel features of the proliferative response of human neuroblastoma cells to 50 Hz magnetic field

Falone S. [*], Santini S. Jr[*], Cacchio M.[#], Di Loreto S.[+], Amicarelli F.[*]

[*]*University of L'Aquila, L'Aquila, Italy;*[#]*University "G. d'Annunzio", Chieti, Italy;* [+]*Institute of Translational Pharmacology - National Research Council (CNR), L'Aquila, Italy*

***Summary* — A continuous exposure to a 50 Hz, 1 mT extremely low frequency magnetic fields (ELF-MF) induced a time-dependent perturbation in cellular biology in human neuroblastoma cells, and promoted conditions commonly associated with more malignant phenotypes and probable chemoresistance.**

I. Introduction

Extremely low frequency magnetic fields (ELF-MFs) are currently classified as "possibly carcinogenic to humans" (1). Human neuroblastoma cells chronically exposed ELF-MF undergo a cytoproliferative response and express new proteins likely linked to enhanced antioxidant defense and undifferentiated status (2). By overexpressing the glyoxalase system, tumors are well protected against methylglyoxal (MG), a dicarbonyl compound mainly produced by glycolysis, the main energy source on which cancer cells rely (3). MG is cytotoxic through the promotion of dicarbonyl and oxidative stress (4, 5). So far, ELF-MF-induced changes in energy metabolism and in cellular defense towards MG are still unknown. We investigated whether the strong proliferative response induced by ELF-MF on neuro-derived SH-SY5Y cells could be linked to re-programming of cellular metabolism and changes in the activity of detoxification systems against MG.

II. Materials and Methods

The sinusoidal 50Hz, 1mT ELF-MF was generated through a copper-wired solenoid (2, 6). Cells were cultured and processed for viable cell counting as described previously (2). The concentration of exogenous MG (400µM) was chosen following concentration-response curves. Lipid peroxidation and GSH were measured photometrically (7, 8), enzymatic activities were measured spectrophotometrically (9-16), arg-pyrimidine, pCREB, pERK1/2 and b(III)-tubulin were measured through immunoblotting (17-19). ANOVA and appropriate post-hoc tests were used for inferential statistics (*P<0.05, **P<0.01, ***P<0.001 vs time-matched controls).

III. Results & Discussion

The early cytoproliferative response (not shown, see Falone et al., 2011) and the reduced level of neuron-specific marker (Fig. 1) indicated a less differentiated phenotype induced by ELF-MF. The early proliferation was linked to the activation of the CREB/ERK-related pathway (Fig. 2), as suggested by others (20). However, CREB-ERK resulted not activated after 10 and 15 days of exposure, thus suggesting that other pathways are involved in sustaining the cytoproliferative response to longer exposures to ELF-MF (fig. 2). We showed for the first time that the MF-induced proliferative effect in SH-SY5Y cells was followed by energy balance re-programming. After an initial activation of the glycolytic pathway and a depression of mitochondrial aerobic activity (5 days), a decreased glycolytic flux and a near-significant increase of the mitochondrial pathway activity were revealed after 15-day exposure (Fig. 3), and this shift was confirmed by the analysis of the protein levels of peroxisome proliferator-activated receptor-gamma coactivator-1alpha (PGC-1α) (Fig. 4). We also found that after an initial pro-oxidant effect, the ELF-MF treatment increased the amount of reduced GSH (Fig. 6), though not through an activation of GSSG recycling pathway (not shown). Moreover, the long-term ELF-MF exposure reduced the lipid peroxidative damage (-40% vs. CTR, Fig. 5) and increased catalase- and glutathione peroxidase-based antioxidant activities (not shown), thus confirming our previous findings (2). In chronically-exposed cells we observed increased MG-targeting detoxification capacities, along with improved removal of MG precursors and reduced MG-related protein damage; coherently, cells exposed to MF for 15 days resulted much more resistant against toxic concentrations of exogenous MG (Fig. 6). However, 5-day ELF-MF treated cells exhibited increased MG-related damage, reduced MG scavenging efficiency and more vulnerability towards MG cytotoxicity (Fig. 6).

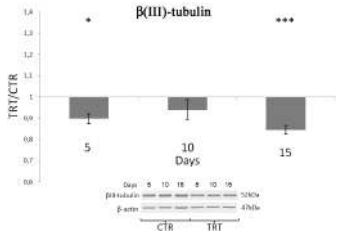

Fig. 1 Differentiative status of SH-SY5Y cells exposed to ELF-MF

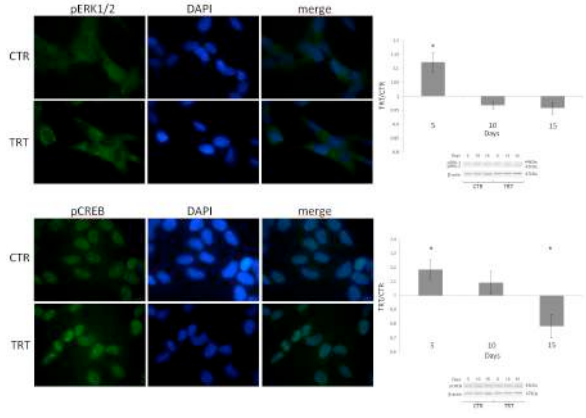

Fig. 2 Immunolocalization (left) and Western blots (right) of pERK1/2 and pCREB in SH-SY5Y cells exposed to ELF-MF for 5 days

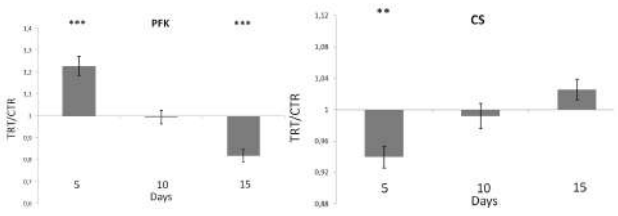

Fig. 3 Glycolytic (PFK, phosphofructokinase) and mitochondrial (CS, citrate synthase) activities in SH-SY5Y cells exposed to ELF-MF

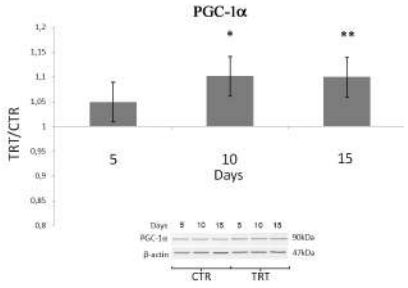

Fig. 4 Mitochondrial biogenesis in SH-SY5Y cells exposed to ELF-MF (PGC-1α, peroxisome proliferator-activated receptor-gamma coactivator-1α)

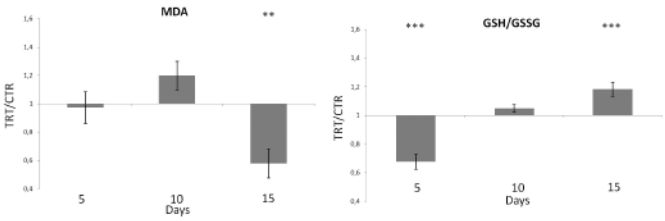

Fig. 5 Lipid peroxidative damage (left) and glutathione redox balance (right) in SH-SY5Y cells exposed to ELF-MF (MDA, malondialdehyde; GSH, reduced glutathione; GSSG, oxidized glutathione).

IV. Conclusions

A 15-day exposure of SH-SY5Y cells to 50Hz, 1mT ELF-MF promoted a complex perturbation in cellular biology, leading to conditions commonly associated with more malignant phenotypes and chemoresistance. Interestingly, this response was time-dependent, being achieved after an early pro-oxidant imbalance, increased glycolytic flux, higher molecular damage and lower resistance against MG.

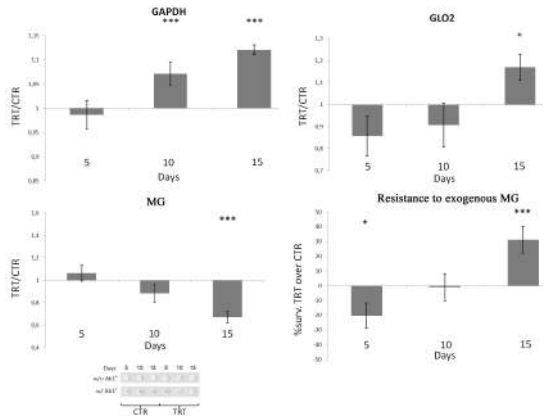

Fig. 6 Removal activity of MG (upper, right) and glycolytic precursors of MG (upper, left). MG-dependent protein damage (lower, left) and cell survival after 24h incubation with toxic concentration of exogenous MG (lower, right).

References

[1] International Agency for Cancer Research (World Health Organization), "*Non-ionizing radiation, part 1: static and extremely-low frequency (ELF) electric and magnetic fields*", Lyon, France: IARCPress, 2002.

[2] S. Falone, M. Sulpizio, F. Amicarelli, M. Marchisio, F. Di Giuseppe, E. Eleuterio, C. Di Ilio and S. Angelucci, "Molecular basis underlying the biological effects elicited by extremely low-frequency magnetic field (ELF-MF) on neuroblastoma cells", *J Cell Biochem*., vol. 112(12), pp. 3797-3806, Dec 2011.

[3] P.J. Thornalley and N. Rabbani, "Glyoxalase in tumourigenesis and multidrug resistance", *Semin Cell Dev Biol*., vol. 22(3), pp. 318-325, May 2011.

[4] F. Amicarelli, S. Colafarina, F. Cattani, A. Cimini, C. Di Ilio, M.P. Ceru and M. Miranda, "Scavenging system efficiency is crucial for cell resistance to ROS-mediated methylglyoxal injury", *Free Radic Biol Med*., vol. 35(8), pp. 856-871, Oct 2003.

[5] S. Di Loreto, V. Zimmitti, P. Sebastiani, C. Cervelli, S. Falone and F. Amicarelli, "Methylglyoxal causes strong weakening of detoxifying capacity and apoptotic cell death in rat hippocampal neurons", *Int J Biochem Cell Biol*., vol. 40(2), pp. 245-257, 2008.

[6] S. Falone, M.R. Grossi, B. Cinque, B. D'Angelo, E. Tettamanti, A. Cimini, C. Di Ilio and F. Amicarelli, "Fifty hertz extremely low-frequency electromagnetic field causes changes in redox and differentiative status in neuroblastoma cells", *Int J Biochem Cell Biol*., vol. 39(11), pp. 2093-2106, 2007.

[7] K. Yagi, "Simple assay for the level of total lipid peroxides in serum or plasma", *Methods Mol Biol*., vol. 108, pp. 101-106, 1998.

[8] M.A. Baker, G.J. Cerniglia and A. Zaman, "Microtiter plate assay for the measurement of glutathione and glutathione disulfide in large numbers of biological samples", *Anal Biochem*., vol. 190(2), pp. 360-365, Nov 1990.

[9] D.E. Paglia and W.N. Valentine, "Studies on the quantitative and qualitative characterization of erythrocyte glutathione peroxidase", *J Lab Clin Med*., vol. 70(1), pp. 158-169, Jul 1967.

[10] P.A. Srere, "Citrate synthase" in: "Methods in Enzymology" (J.M. Lowenstein, Ed.), vol. 13, pp. 3-11, 1969.

[11] H.U. Bergmeyer, K. Gawehn and M. Grassl, in: "Methods of Enzymatic Analysis - 2nd edition" (H.U. Bergmeyer, Ed.), vol. 1, pp. 466-467, New York, NY, USA: Academic Press, Inc., 1974.

[12] M. Sun and S. Zigman, "An improved spectrophotometric assay for superoxide dismutase based on epinephrine autoxidation", *Anal Biochem*., vol. 90(1), pp. 81-89, Oct 1978.

[13] C. Di Ilio, G. Polidoro, A. Arduini, A. Muccini, G. Federici, "Glutathione peroxidase, glutathione reductase, glutathione S-transferase, and gamma-glutamyltranspeptidase activities in the human early pregnancy placenta", *Biochem Med*., vol. 29(2), pp. 143-148, Apr 1983.

[14] H. Aebi, "Catalase in vitro", *Methods Enzymol*., vol. 105, pp. 121-126, 1984.

[15] M.K. Guha, D.L. Vander Jagt and D.J. Creighton, "Diffusion-dependent rates for the hydrolysis reaction catalyzed by glyoxalase II from rat erythrocytes", *Biochemistry*, vol. 27(24), pp. 8818-8822, Nov 1988.

[16] B. Sharma, S. Ghatak, O.P. Malhotra and N.A. Kausha, "Stabilisation and characterisation of phosphofructokinase purified from Setaria cervi, a bovine filarial parasite". *Helminthologia*, vol. 32, pp. 15–23, 1995.

[17] U.K. Laemmli, "Cleavage of structural proteins during the assembly of the head of bacteriophage T4", *Nature*, vol. 227(5259), pp. 680-685, Aug 1970.

[18] H. Towbin, T. Staehelin, J. Gordon, "Electrophoretic transfer of proteins from polyacrylamide gels to nitrocellulose sheets: procedure and some applications", *Proc Natl Acad Sci USA*, vol. 76(9), pp. 4350-4354, Sep 1979.

[19] S. Falone, A. D'Alessandro, A. Mirabilio, G. Petruccelli, M. Cacchio, C. Di Ilio, S. Di Loreto and F. Amicarelli, "Long term running biphasically improves methylglyoxal-related metabolism, redox homeostasis and neurotrophic support within adult mouse brain cortex", *PLoS One*, vol. 7(2), pp. e31401, 2012.

[20] M.A. Martínez, A. Úbeda, M.A. Cid and M.Á. Trillo, "The proliferative response of NB69 human neuroblastoma cells to a 50 Hz magnetic field is mediated by ERK1/2 signaling", *Cell Physiol Biochem*., vol. 29(5-6), pp. 675-686, 2012.

A Low-Frequency Electromagnetic (LF-EMF) Exposure Scheme Induces Autophagy Activation to Counteract in Vitro Aβ-Amyloid Neurotoxicity

Federico Manai[1], Lorenzo Fassina[2,3], Letizia Venturini[4], Francesca Angeletti[1], Cecilia Osera[5], Nicoletta Marchesi[5], Marialaura Amadio[5], Alessia Pascale[5], Giovanni Ricevuti[4], Sergio Comincini[1], Salvatore Caorsi[2,6]

1Department of Biology and Biotechnology, University of Pavia, 27100 Pavia, Italy

2Department of Industrial and Information Engineering, University of Pavia, 27100 Pavia, Italy

3Centre for Tissue Engineering (C.I.T.), University of Pavia, 27100 Pavia, Italy

4IDR "Santa Margherita", Department of Internal Medicine and Therapeutics, Section of Geriatrics and Gerontology, University of Pavia, 27100 Pavia, Italy

5Department of Drug Sciences, Section of Pharmacology, University of Pavia, 27100 Pavia, Italy

6Research Unit ICEMB, University of Pavia, 27100 Pavia, Italy, salvatore.caorsi@unipv.it

***Summary*—A low frequency electromagnetic field (LF-EMF) scheme was developed to increase the clearance capability of neurotoxic Aβ amyloid peptides *in vitro*. Specifically, LF-EMF activates endogenous autophagic pro-survival effects resulting in the autophagosome engulfment of the toxic protein aggregates. These results might address novel therapeutic strategies for neurodegenerative diseases.**

I. Introduction

Epidemiological studies have shown a correlation between LF-EMF exposure and an increased risk to develop several diseases, including tumors and neurodegenerative disorders [1]. However, EMF can also elicit positive effects on biological systems; certain types of EMF are indeed currently employed in clinical practice to treat different dysfunctions. For instance, a pioneering field of research in Alzheimer's disease (AD) is the deep brain stimulation via EMF, which seems to produce clinical benefits in AD patients [2]. Autophagy is a multi-step lysosomal degradation process able to maintain cellular homeostasis through the digestion of long-lived proteins and damaged organelles [3]. The process of autophagy involves the formation of double membrane vesicles (autophagosomes) that engulf organelles and cytoplasm, and finally fuse with the lysosome to form the autolysosomes, where the contents are degraded. Defects in autophagosome formation and loss of basal autophagy may be implicated as a cause of neurodegeneration [4], while an increased autophagic activity may help to clear key aggregated proteins involved in neurodegenerative pathologies. There is also mounting evidence that if the autophagosome-lysosomal degradation is impaired, this could disturb the processing of APP and participate to the development of AD pathology [5].

In this context, we have recently reported the effect of a pulsed LF-EMF (frequency of 75 Hz, magnetic field intensity equal to 2 mT, pulse duration of 1.3 ms) exposure scheme on a specific microRNA sequence that in turn regulates the expression of an autophagy-regulatory gene, finally inducing the activation of the autophagy process in human neuroblastoma cells [6].

II. Methods

A. Cell culture, autophagy and Aβ–amyloid visualization

Human neuroblastoma SH-SY5Y cells (ATCC) were grown in DMEM High glucose medium at 37°C, 5% CO_2. The cultured cells were subjected to LF-EMF by placing the appropriate multiwell plates or petri dishes within the electromagnetic bioreactor and exposing the cells to the below described stimulus. For autophagy evaluations in living cells, SH-SY5Y cells were transduced with BacMam LC3B-GFP expressing viral vector as described [6] or alternatively visualized using acridine orange staining (1 μM for 15 min.). To evaluate LF-EMF effects in counteracting $A\beta_{1\text{-}42}$ amyloid mediated toxicity, the peptides (1 μM, Sigma-Aldrich), were added to SH-SY5Y cells before the LF-EMF treatments. Autofluorescent $A\beta_{1\text{-}42}$ peptides were visualized by inverted microscope at 330 nm and LC3B-GFP at 480 nm excitations, respectively in living cells.

B. Electromagnetic bioreactor

The pulse generator used was provided by Igea (Carpi, Italy) and powered the electromagnetic bioreactor previously described [7] with the following parameters: intensity of the magnetic field (2±0.2 mT), amplitude of the induced electric

tension (5±1 mV), signal frequency (75±2 Hz), and pulse duration (1.3 ms). The experiments were performed with 1 hour LF-EMF duration and different recovery post-treatment (p.t.) times were investigated. Control cultures were placed into an identical incubator in the absence of LF-EMF stimulation.

III. RESULTS AND DISCUSSION

As recently reported [6] and additionally illustrated in Figure 1, SHSY-5Y cells exposed to LF-EMF for 1 hour, exhibited a significant increase in autophagic vesicles, without negative effects on their viability rates. We therefore assayed these cells to endogenous Aβ-amyloid peptides (i.e. $A\beta_{1-42}$ at 1 μM) using a concentration that not directly induce irreversible damages or cell death.

As an initial approach we incubated cells directly with non-fluorescent $A\beta_{1-42}$ peptides, and exposed or not- to the specific LF-EMF scheme. After additional 24 hours p.t., as reported in Figure 2, autofluorescent peptides were visible as discrete cytoplasmic and perinuclear spots, without showing difference in distribution between LF-EMF treated and untreated cells. To better localize these intracellular aggregates, cells were again exposed or not- to the specific LF-EMF scheme and transduced with a baculovirus vector (BacMam) expressing the LC3B-GFP autophagic marker. As a result, a significant degree of co-localization of autofluorescent $A\beta_{1-42}$ aggregate peptides and autophagic vescicles was scored in LF-EMF treated cells compared to untreated ones (Figure 3).

In conclusion, these results highlighted that a specific LF-EMF scheme can significantly increase the intracellular content of autophagic vesicles without affecting their viability and that these vesicles can contribute to the clearance of Aβ-amyloid peptides, thus suggesting a potential novel therapeutic strategies within neurodegenerative diseases like Alzheimer's.

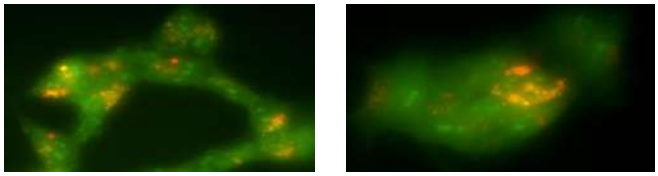

Fig. 1 Fluorescent microscope evaluation of autophagic vescicles in SHSY-5Y living cells using acridine orange staining after LF-EMF 1 hour exposition (left) or by incubation with the autophagic inducer Rapamycyn (1 mM) (right). Cells were observed at 24 hours p.t.; acidic vesicles are stained in red, while not-acidic ones in yellow.

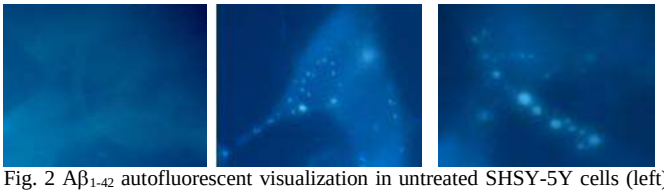

Fig. 2 $A\beta_{1-42}$ autofluorescent visualization in untreated SHSY-5Y cells (left), cells incubated with $A\beta_{1-42}$ (1 μM) and exposed to LF-EMF for 1 hour (center) and cells incubated with $A\beta_{1-42}$ (1 μM) but not exposed to LF-EMF. Cells were observed at 24 hours p.t

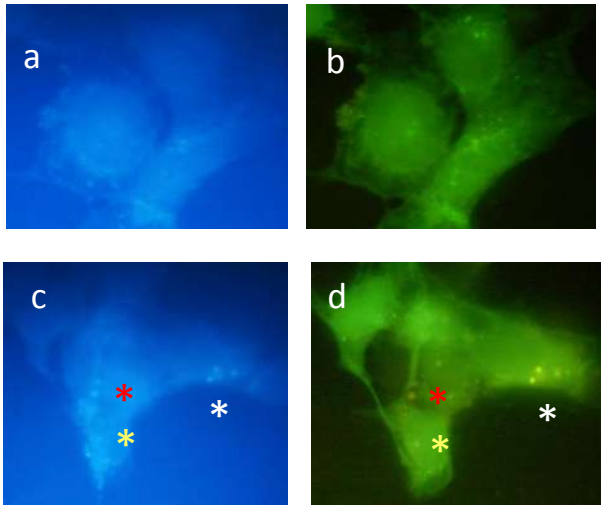

Fig. 3 $A\beta_{1-42}$ autofluorescent visualization in untreated (a) or after 1 hour LF-EMF treatment (c) SHSY-5Y cells both incubated with $A\beta_{1-42}$ (1 μM). (b) and (d) are corresponding fluorescent panels of cells transduced with BacMam LC3-GFP. Asterisks with different colors indicated co-localized $A\beta_{1-42}$–LC3B autophagosome signals, mostly scored after LF-EMF exposition. Cells were observed at 24 hours p.t.

IV. BIBLIOGRAPHY

[1] Z. Davanipour, C. C. Tseng, P. J. Lee, and E. Sobel, 2007 "A case-control study of occupational magnetic field exposure and Alzheimer's disease: results from the California Alzheimer's Disease Diagnosis and Treatment Centers," BMC Neurology, vol. 7, pp.13, 2007.

[2] A. W. Laxton, D. F. Tang-Wai, M. P. McAndrews, D. Zumsteg, R. Wennberg, R. Keren, J. Wherrett, G. Naglie, C. Hamani, G. S. Smith, and A. M. Lozano, "A Phase I Trial of Deep Brain Stimulation of Memory Circuits in Alzheimer's Disease," Annals of Neurology, vol. 68, pp. 521-534, 2010.

[3] K.N. Dalby, I. Tekedereli, G. Lopez-Berestein, and B. Ozpolat, "Targeting the prodeath and prosurvival functions of autophagy as novel therapeutic strategies in cancer," Autophagy, vol. 6, pp. 322-329, 2010.

[4] E. Wong Eand A. M. Cuervo, "Autophagy gone awry in neurodegenerative diseases," Nature Neuroscience, vol. 13, pp. 805-811, 2010.

[5] A. Salminen, K. Kaarniranta, A. Kauppinen, J. Ojala, A. Haapasalo, H. Soininen, and M. Hiltunem, "Impaired autophagy and APP processing in Alzheimer's disease: The potential role of Beclin 1 interactome," Progress in Neurobiology, vol. 106, pp. 33-54, 2013.

[6] N. Marchesi, C. Osera, L. Fassina, M. Amadio, F. Angeletti, M. Morini, G. Magenes, L. Venturini, M. Biggiogera, G. Ricevuti, S. Govoni, S. Caorsi, A. Pascale, and S. Comincini, "Autophagy Is Modulated in Human Neuroblastoma Cells Through Direct Exposition to Low Frequency Electromagnetic Fields," Journal of Cellular Physiology 2014.

[7] L. Fassina, L. Visai, F. Benazzo, L. Benedetti, A. Calligaro, M. G. C. De Angelis, A. Farina, V. Maliardi, and G. Magenes, "Effects of electromagnetic stimulation on calcified matrix production by SAOS-2 cells over a polyurethane porous scaffold," Tissue Engineering, vol. 12, pp.1985-1999, 2006.

Pulsed electromagnetic field prevents H_2O_2-induced reactive oxygen species production by increasing MnSOD activity in SK-N-BE neuronal cells

Marchesi Nicoletta[1]*, Amadio Marialaura[1]*, Falone Stefano[2], Osera Cecilia[1], Fassina Lorenzo[3,4], Magenes Giovanni[3,4], Comincini Sergio[5], Caorsi Salvatore[3,6], Amicarelli Fernanda[2], Ricevuti Giovanni[7], Govoni Stefano[1], Pascale Alessia[1]

[1] *Department of Drug Sciences, Section of Pharmacology, University of Pavia, 27100 Pavia, Italy*
[2] *Department of Life, Health and Environmental Sciences, University of L'Aquila, 67100 L'Aquila, Italy*
[3] *Department of Industrial and Information Engineering, University of Pavia, 27100 Pavia, Italy*
[4] *Centre for Tissue Engineering (C.I.T.), University of Pavia, 27100 Pavia, Italy*
[5] *Department of Biology and Biotechnology, University of Pavia, 27100 Pavia, Italy*
[6] *Research Unit ICEMB, University of Pavia, 27100 Pavia, Italy,*
[7] *IDR "Santa Margherita", Department of Internal Medicine and Therapeutics, Section of Geriatrics and Gerontology, University of Pavia, 27100 Pavia, Italy*

**These authors equally contributed to this work*

***Summary*— We investigated the effects of short and repeated pulsed electromagnetic fields (PEMF; magnetic field intensity 2 mT, frequency 75 Hz) on SK-N-BE neuronal cells. The results show that PEMF stimulation elevated the MnSOD activity, thus counteracting the effects of a H_2O_2-based pro-oxidant challenge.**

I. Introduction

Extremely low frequency electromagnetic fields (ELF-EMF, 1-300 Hz) emitted by domestic and industrial appliances are widespread worldwide. To this regard, some epidemiological and occupational studies have shown a correlation between ELF-EMFs exposure and an increased risk of developing some diseases, including tumors (*e.g.* leukemia) [1] or neurodegenerative disorders such as Alzheimer's disease (AD) [2]. Specifically, PEMF (Pulsed Electromagnetic Fields) stimulation has been employed in bone repair and regeneration [3], and in the treatment of different types of pain [4]. In general, it can be stated that ELF-EMF-induced effects can be either cytotoxic or cytoprotective in a time- and dose-dependent way [5,6]. In addition, biological responses elicited by EMF can be function of the responsiveness of the cell type, tissue or organism investigated [7]. The cytoprotection might be induced by a kind of "hormetic effect", in which low doses of otherwise adverse chemical/physical stimuli improve the "functional ability" of cells and tissues to face noxae. To this regard, based on the concept that the hormetic effect may implicate the strengthening of the molecular responses towards stress, it has been proposed the use of ELF-EMF as a possible therapy against neurodegenerative disorders, such as AD, as documented by the delay of the cellular senescence associated with an increased expression of heat shock proteins [8]. Here we demonstrated that in a human neuroblastoma cell line (SK-N-BE) a repeated stimulation with non-toxic short PEMF (magnetic field intensity 2 mT, frequency 75 Hz) positively affects the cellular response against a pro-oxidant chemical insult such as H_2O_2. H_2O_2 challenge determines a reduction in intracellular reactive oxygen species (ROS) production in PEMF-treated neuroblastoma cells, and an increase of MnSOD activity.

II. Materials and Methods

A. Cell cultures

SK-N-BE human neuroblastoma cells were grown in Eagle's minimum essential medium (MEM), supplemented with 10% fetal bovine serum, 1% penicillin-streptomycin, L-glutamine (2 mM), non-essential amino acids (1 mM), and sodium-pyruvate (1 mM), at 37°C in an atmosphere of 5% CO_2 and 95% humidity.

B. Electromagnetic bioreactor and cell treatments

An electromagnetic bioreactor was built as previously described [9]. The electromagnetic bioreactor applied to the cells a PEMF with the following characteristics: intensity of the magnetic field equal to 2 ± 0.2 mT, amplitude of the induced electric tension equal to 5 ± 1 mV, signal frequency of 75 ± 2 Hz, and pulse duration of about 1.3 ms. The cultured cells were subjected to PEMF for 72 h, 30 min, 15 min exposure and they underwent a total of 3 treatments over 5 days. The control cultures were placed into a different incubator in the absence of PEMF stimulation. 24 h after the last PEMF stimulation, exposed and not-exposed cells were treated with 1 mM H_2O_2 (Sigma-Aldrich) for 10 or 30 min.

C. MTT assay

Mitochondrial function was estimated by using the MTT [3-(4,5-dimethylthiazol-2-yl)-2,5-diphenyltetrazolium bromide] assay (Sigma-Aldrich), as previously described [9]. Absorbance values were measured at 595 nm in a microplate reader (model 550; Bio-Rad Laboratories) and results expressed as absorbance$\times 10^3$.

D. Detection of reactive oxygen species

ROS formation was measured by using the fluorescent probe 2',7'-dichlorofluorescein diacetate (DCFH-DA; VWR International PBI) which forms 2',7'-dichlorofluorescein (DCF) when oxidized by ROS. Briefly, SK-N-BE cells were seeded and after H_2O_2 treatment cells were loaded with 10 μM

DCFH-DA and placed in the incubator for 30 min. At the end of the incubation, the fluorescent intensity was measured with SpectraMax Gemini XS spectrofluorometer (excitation 485 nm, emission 530 nm) (Molecular Devices). Data were expressed as a percentage with reference to the control.

E. Tissue homogenates preparation for superoxide dismutase activity

Control and treated SK-N-BE cells were harvested and suspended in 0.1 M phosphate buffer containing 0.1% (v/v) Triton X-100. The cell suspension was used for spectrophotometrical measurement of enzymatic activity and protein content to study the activity of the total superoxide dismutase (SOD) (EC 1.15.1.1) and to discriminate between the copper–zinc (SOD1) and the manganese-containing (SOD2) superoxide dismutase enzyme activities, as previously described [10].

F. Statistics

Datasets were analyzed by the analysis of variance (ANOVA) followed by appropriate *post-hoc* test. Differences were considered statistically significant when $p<0.05$.

II. Results and Discussion

PEMF pre-treatment of SK-N-BE cells stimulated MnSOD activity and counteracted H_2O_2-induced ROS production

A 72 h exposure to PEMF significantly decreased the mitochondrial function in SK-N-BE cells (-17%; $p<0.0001$). SK-N-BE cells were exposed to short PEMF stimuli for 1 h, 30 or 15 min, repeated 3 times over a period of 5 days (for a total of 3 h, 90 min or 45 min PEMF stimulation, respectively).

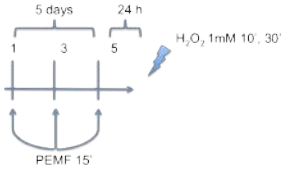

Figure 1: Scheme of the experimental protocol in SK-N-BE cells, where PEMF treatment was followed by a 1 mM H_2O_2 challenge of 10 and 30 min.

Since the 15 min exposure did not cause any change in mitochondrial activity, this experimental protocol was adopted for all the subsequent experiments. In order to assess whether the PEMF pre-exposure was able to modify the cellular response to H_2O_2, 24 h after the last PEMF exposure SK-N-BE cells were treated with 1 mM H_2O_2 for 10 or 30 min. In cells not exposed to PEMF, 10 and 30 min H_2O_2 treatments cause a small but significant decrease in mitochondrial activity; interestingly, this parameter was not affected in cells pre-exposed to PEMF, neither after H_2O_2 exposure (data not shown).

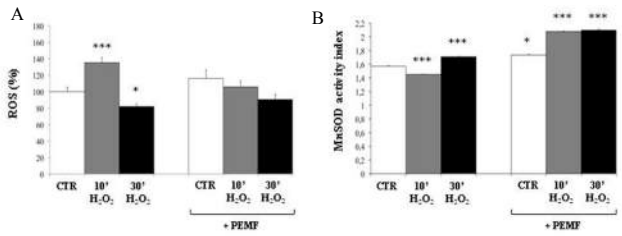

Figure 2: (A) ROS production expressed as mean ± SEM. Values indicate fluorescence intensity as a percentage over control (100%). (n=18). (B) Mean ± SEM of MnSOD activity expressed as MnSOD activity index. *$p<0.05$, , ***$p<0.0001$, Dunnett Multiple Comparisons test (n=3).

In non-exposed cells, the 10-min H_2O_2 stimulus increased ROS production, which was instead decreased 30 min after the oxidative challenge. In parallel, MnSOD activity was found significantly decreased following 10 min of H_2O_2 and increased after 30 min H_2O_2 treatment (Fig. 2). It is presumable that cells respond to the 30 min oxidative challenge by increasing MnSOD protein activity, thus restoring ROS basal levels. Interestingly, PEMF-treated cells showed higher MnSOD basal activity when compared to non-exposed cells, and this enzymatic activity further increased after 10 and 30 min exposure with H_2O_2. SK-N-BE cells pre-treated with the PEMF showed unchanged ROS basal levels when compared to non-exposed cells. Moreover, the H_2O_2 treatment did not cause significant changes in ROS production in PEMF pre-exposed cells, although a trend in ROS reduction was detected (Fig. 2).

Our findings suggest that a repeated PEMF pre-exposure (for a total of 45 min) could be beneficial for SK-N-BE neuroblastoma cells, in which a cytoprotective response was observed; indeed, they respond by increasing MnSOD activity to counteract ROS production. The described effects could be indicative of a possible hormetic use of PEMF stimulation to improve the functional ability of neuroblastoma cells and protecting the cells from a noxious agent.

Bibliography

1. Kheifets, L. *et al.;* Pooled analysis of recent studies on magnetic fields and childhood leukaemia. *Br. J. Cancer* 103:1128-1135; 2010.
2. Davanipour, *Z. et al.;* A case-control study of occupational magnetic field exposure and Alzheimer's disease: results from the California Alzheimer's Disease Diagnosis and Treatment Centers. *BMC. Neurol.* **7:**13; 2007.
3. Fassina, L. *et al.;* Ultrasonic and electromagnetic enhancement of a culture of human SAOS-2 osteoblasts seeded onto a titanium plasma-spray surface. *Tissue Eng Part C. Methods* **15:**233-242; 2009.
4. Rohde, C. et al.; Effects of pulsed electromagnetic fields on interleukin-1 beta and postoperative pain: a double-blind, placebo-controlled, pilot study in breast reduction patients. *Plast. Reconstr. Surg.* **125:**1620-1629; 2010.
5. Carmody, S. et al.; Cytoprotection by electromagnetic field-induced HSP70: a model for clinical application. *J. Cell Biochem.* **79:**453-459; 2000.
6. Gobba, F. et al.; Natural killer cell activity decreases in workers occupationally exposed to extremely low frequency magnetic fields exceeding 1 microT. *Int J. Immunopathol. Pharmacol.* **22:**1059-1066; 2009.
7. Simko, M. et al.; Cell type specific redox status is responsible for diverse electromagnetic field effects. *Curr. Med. Chem.* **14:**1141-1152; 2007.
8. Cotelli, M. et al.; Improved language performance in Alzheimer disease following brain stimulation. *J. Neurol. Neurosurg. Psychiatry* **82:**794-797; 2011.
9. Osera, C. et al.; Cytoprotective response induced by electromagnetic stimulation on SH-SY5Y human neuroblastoma cell line. *Tissue Eng Part A* **17:**2573-2582; 2011.
10. Paynter, D.I.; Changes in activity of the manganese superoxide dismutase enzyme in tissues of the rat with changes in dietary manganese. *J Nutr*. **110:**437-447; 1980.

Pulsed Electromagnetic Fields Stimulate Osteogenic Differentiation in Human Bone Marrow and Adipose Tissue Derived Mesenchymal Stem Cells

Alessia Ongaro[*], Agnese Pellati[*], Leila Bagheri[*], Cinzia Fortini[+], Monica De Mattei[*]

[*]*Department of Morphology, Surgery and Experimental Medicine, University of Ferrara, Via Fossato di Mortara 70, 44121 Ferrara, Italy; alessia.ongaro@unife.it, pllgns@unife.it; leila.bagheri@student.unife.it, dmm@unife.it*

[+]*Chair of Cardiology, University of Ferrara, Via Fossato di Mortara 70, 44121 Ferrara, Italy; cinzia.fortini1@unife.it*

***Summary*— PEMFs have a stimulatory role in osteogenesis of human mesenchymal stem cells derived from bone marrow and adipose tissue, independently from the presence of bone morphogenetic protein-2. PEMFs may be considered a tool to improve autologous cell-based regeneration of bone defects in orthopedics.**

I. Introduction

Mesenchymal stem cells (MSCs) derived from different sources like bone marrow and adipose tissue have been extensively used in the research field of bone cell therapy and tissue engineering. Although bone marrow is considered as an enriched source of MSCs, the isolation procedure is invasive for donors and patients. For this reason, the identification of multipotent precursor cells from human liposuction aspirates, known as adipose derived mesenchymal stem cells (ASCs) has stimulated a growing interest in adult stem cells research. Compared with stem cells isolated from bone marrow (BMSCs), ASCs are easier to obtain, available in larger amount and proliferate rapidly, providing an attractive cell source for clinical application. Studies comparing the differentiation capacity of BMSCs and ASCs have found that both cell types can differentiate into ostegenic lineage, although ASCs showed a less osteogenic differentiation potential than BMSCs [1].

Several in vitro, in vivo and clinical studies have shown that biophysical stimulation with pulsed electromagnetic fields (PEMFs) plays a regulatory role of connective tissue, particularly bone, cartilage, synovia by stimulating cell proliferation, extracellular matrix production, and inhibiting inflammatory activities [2]. In vitro studies have indicated that PEMFs may stimulate osteoblast proliferation, matrix organic component production and mineralization. Furthermore, PEMFs can influence the behaviour of BMSCs, particularly their differentiation into the osteogenic lineage [3]. The effect of PEMFs on ASCs osteogenic differentiation has been only recently investigated and it has been found that the expression of osteogenic markers was enhanced by PEMF treatment [4].
Bone morphogenetic protein (BMP)-2, belonging to TGF-β superfamily, strongly promote osteoblast differentiation. Notably, it has been reported that BMP-2 exerts a synergistic action with PEMFs to induce osteogenic differentiation in BMSCs [3].

The aim of our study was to evaluate whether biophysical stimulation with PEMFs may favor osteogenic differentiation both in BMSCs and also in ASCs and to compare the role of PEMFs alone and in combination with BMP-2. To this purpose, we analysed at different time points (3, 7, 11, 14, 21 and 28 days) the role of PEMFs on ALP activity, osteocalcin levels and matrix mineralization, that are considered respectively early and later osteogenic markers.

II. Materials and Methods

A. Cell Cultures

Human BMSCs were purchased from Lonza (Walkersville, MD, USA). Adipose tissue was obtained by liposuction from abdominal subcutaneous fat of healthy donors after written consent and Institutional Review Board approval. Adipose tissue was digested with collagenase I (Sigma Aldrich, St. Louis, MO,USA), and plated in dishes in mesencult medium (StemCell Technologies, Vancouver, Canada). Expression of typical mesenchymal markers (CD14, CD29, CD34, CD44, CD45, CD73, CD90 and CD105) was verified on cultures at third passage on ASCs by flow cytometry analysis.

BMSCs and ASCs at third passage were seeded at an initial density of 2.5×10^3 cells/cm^2 in 4-well plates (Nunc, Roskilde, Denmark) and were cultured for 28 days in 1ml of appropriate culture medium in the following treatment groups:

- Control: cells were cultured in expansion media to obtain undifferentiated control cells (data not shown);
- Osteogenic Medium (OM): cells were cultured in OM to induce osteogenic differentiation;
- BMP-2: cells were cultured in OM in the presence of 50 ng/ml BMP-2.

All medium were from Lonza. BMP-2 was from PeproTech, London, UK.

B. Characteristics of PEMF and exposure conditions

The PEMF generator system consisted of a pair of circular Helmoltz coils of copper wire, placed opposite to each other, and in a signal generator (IGEA S.p.a., Carpi, Italy). The cell plates were placed between the pair of Helmoltz coils. The power generator produced a pulsed signal with pulse duration of 1.3 ms and frequency of 75 Hz, yielding a duty cycle of 1/10. The peak value of the magnetic field was 1.5 mT. The shape of the induced electric field and its impulse length were kept constant. In PEMF exposed cells, the PEMF exposure was maintained for the whole differentiation time (28 days).

C. Osteogenic markers

The alkaline phosphatase (ALP) activity was determined on cellular lysates in the presence of p-nitrophenylphosphate (p-NP) (Sigma). The reaction was stopped with 0.2 M NaOH and the absorbance of each sample was read at 405 nm with a

Spectrophotometer. ALP activity was then normalized to total DNA content and was expressed as nanomolar of p-NP/min/µg DNA.

Osteocalcin (OC) was analyzed using commercial ELISA kit (Invitrogen, Rockville, MD, USA). OC levels were expressed as ng ostocalcin/µg DNA.

Matrix mineralization was visualized by staining cultures, fixed in 70% cold ethanol, with 2% Alizarin red (Sigma) solution (pH 4.1–4.3).

D. Statistical Analysis

All experiments (n=4) were performed in triplicate. The results obtained in the different experimental conditions (in the presence or in the absence of PEMF exposure) in the three groups of cells (Control, OM and BMP-2) were compared through Kruskal–Wallis test.

III. Results

In BMSCs, PEMFs treatment appeared to stimulate earlier the increase of ALP activity in the absence and in the presence of BMP-2 (Fig. 1).

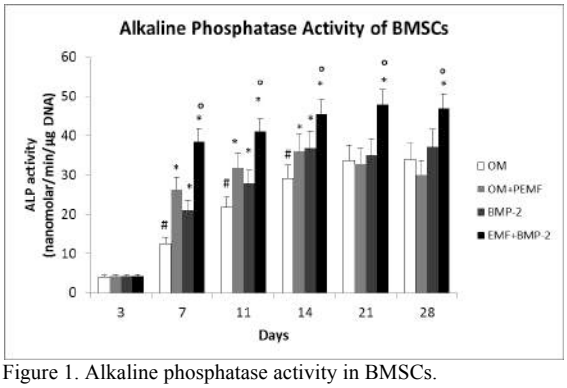

Figure 1. Alkaline phosphatase activity in BMSCs.

Similarly, in ASCs grown in OM alone, although ALP levels were lower than those obtained in BMSCs, PEMFs exposure significantly increased ALP activity with respect to unexposed ASCs. In the presence of BMP-2 in the OM, PEMF exposure further significantly increased the ALP.

The later osteogenic marker OC significantly increased after day 14 in culture. PEMF exposure significantly enhanced the OC levels of 3.8-fold at day 21 and 5.2-fold at day 28 (Fig. 2) compared with PEMF-unexposed BMSCs. The stimulatory effect of PEMFs was further raised by BMP-2 (Fig. 2).

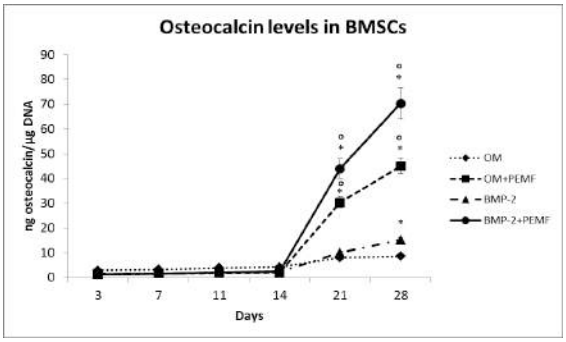

Figure 2. Osteocalcin levels in BMSCs.

In ASCs, PEMFs enhanced the OC levels of 7.7-fold at day 21 and 3.7-fold at day 28, thus anticipating of 7 days the OC production respect to the PEMF-unexposed cells. The addition of BMP-2 in OM did not further increase the OC levels induced by PEMFs in ASCs.

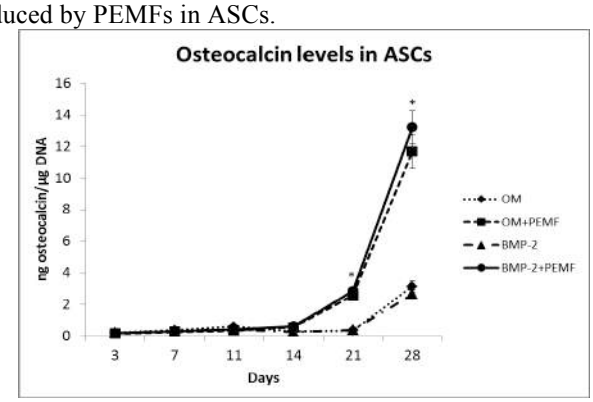

Figure 3. Osteocalcin levels in ASCs.

Also the accumulation of calcium deposits was more consistent in PEMFs exposed BMSCs, both in the absence and in the presence of BMP-2, compared to unexposed cells. Although to a lesser extent respect to BMSCs, also in ASCs matrix mineralization was observed at day 28 with increased calcium deposition in PEMFs exposed ASCs, regardless of the supplementation with BMP-2 in OM.

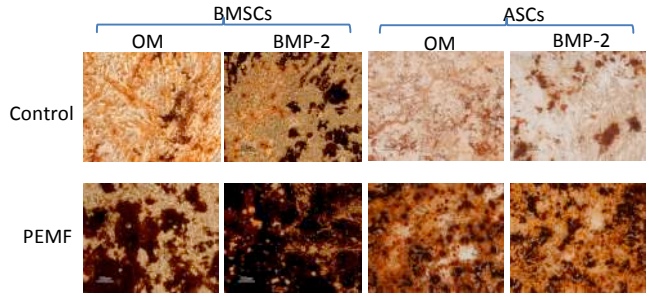

Figure 5. Matrix mineralization in BMSCs and ASCs.

IV. Conclusions

PEMFs favor in vitro osteogenic differentiation in BMSCs and ASCs. The enhancement induced by PEMFs on ALP activity, OC levels and matrix mineralization suggested a PEMF role in early and in later phases of osteogenic differentiation. Notably, the effects of PEMFs were evident not only in BMSCs but also in ASCs. In BMSCs, the PEMF effect was further increased by BMP-2, whilst in ASCs we found a stimulatory effect of PEMFs on the osteogenesis regardless the BMP-2 treatment. These results suggest PEMFs as a possible tool to improve autologous cell-based regeneration of bone defects.

References

[1] Shafiee A, et al., "A comparison between osteogenic differentiation of human unrestricted somatic stem cells and mesenchymal stem cells from bone marrow and adipose tissue", *Biotechnol Lett*, vol 33, pp. 1257–1264, 2011.

[2] Ongaro A, et al., "Chondroprotective effects of pulsed electromagnetic fields on human cartilage explants", *Bioelectromagnetics,* vol. 32, pp. 543–551, 2011.

[3] Schwartz Z, et al., "Pulsed electromagnetic fields enhance BMP-2 dependent osteoblastic differentiation of human mesenchymal stem cells", *J Orthop Res.,* vol. 26, pp. 1250–1255, 2008.

[4] Chen CH, et al., "Electromagnetic fields enhance chondrogenesis of human adipose-derived stem cells in a chondrogenic microenvironment in vitro", *J Appl Physiol*., vol 114, pp. 647–655, 2013.

Effect of Magnetic Field (MF) on Alkaline Phosphatase Activity of Human Osteosarcoma Cells

Rescigno Tania*, Caputo Mariella*, Bisceglia Bruno*, Tecce Mario Felice*[1]

* *Department of Pharmacy, University of Salerno, Via Giovanni Paolo II, 132, 84084 Fisciano (Sa)*

[1] *corresponding author: tecce@unisa.it*

Abstract- We evaluated the effects of a magnetic field (MF) exposure system (75 Hz, 1.5 mT), on human osteosarcoma cells (SaOS-2) cultured in presence or in absence of three-dimensional collagen scaffolds. In both experimental conditions, we found our physical stimulus capable to increase the activity of alkaline phosphatase (ALP), a typical marker of bone regeneration, with no effect on cell vitality.

I. INTRODUCTION

Pulsed electromagnetic fields (PEMFs) have been shown to positively affect osteogenic processes [1-4]. Several works report the ability of PEMFs to affect proliferation and differentiation of bone cells in vitro, to increase the expression of bone marker genes and to induce bone mineralization processes [5-7]. During the last years, biomedical research is giving special interest to the development of biocompatible scaffolds to improve bone surgery. In particular, in the three-dimensional structure of these materials, cells can proliferate, differentiate and release bone extracellular matrix, promoting new tissue generation [8-9]. Alkaline phosphatase (ALP) activity is considered as a marker typically associated to osteogenesis and bone tissue regeneration [10]. Therefore it is usually used to investigate the development of these processes. In this study, we evaluated the effects of a magnetic field (MF) exposure system (75 Hz, 1.5 mT), currently used for the therapeutic treatment of bone injuries to increase tissue regeneration, on a human osteosarcoma cell line (SaOS-2). Cells were exposed to our physical stimulus for 1h in presence or in absence of collagen scaffolds imitating bone tissue organization and, subsequently, cell proliferation and alkaline phosphatase activity were measured 0, 4 and 24 hours after the exposure.

II. METHODOLOGY

A. 3D Scaffolds

Collagen scaffolds employed for our investigation were kindly provided by Finceramica (Faenza, Italy). Scaffolds were produced by a process integrating an organic compound (collagen type I) with bio-active hydroxyapatite nano-crystals with magnesium salts.

B. Magnetic field exposure system and exposure conditions

SaOS-2 cells, attached to the cell culture multiwell (24 wells) or bone scaffold surface and/or loaded into the 3D scaffold structure, were exposed to the magnetic field (75 Hz, 1.5 mT) produced by a device kindly provided by IGEA (Carpi, Italy), for 1h at room temperature. MTT and ALP activity assays were performed 0, 4 and 24 hours after the exposure.

C. MTT and ALP activity assays

The methyl thiazolyl blue tetrazolium (MTT) spectrophotometric dye assay was used to detect cell proliferation ability. Cells were incubated for 2h in 1mL MTT (1mg/mL) at 37°C. Colour was developed by incubating cells in 800 µL dimethyl sulfoxide, and absorbance was detected at 490 nm wave length. The ALP activity assay was performed by a colorimetric reaction. Cells were incubated in a lysis solution containing 0.1% Triton-X 100, 50 mM citric acid (pH 5.5), and 5 mM p-nitrophenyl phosphate (p-NPP), for 45 min at 37°C. During this time, ALP enzyme catalyses the hydrolysis of p-NPP into p-nitrophenol (p-NP). The reaction was stopped with 1 M NaOH and the p-NP production, proportional to the amount of enzyme activity, was evaluated by measuring absorbance at 405 nm wave length.

III. RESULTS AND DISCUSSION

To evaluate cell survival and proliferation on or within collagen scaffolds, we carried out an MTT assay. The measured absorbance resulted proportional to the number of seeded cells and to the time of cell culture (not shown). Results showed that used cells were able to colonize scaffolds and proliferated within their spaces.

Afterwards, we treated cells, both in presence or in absence of scaffolds, with the physical stimulus produced by our MF exposure system for 1h and we found that our magnetic stimulation was able to induce significant increases of alkaline phosphatase activity particularly 4 and 24 hours after the exposure (Fig. 1). The increases are even larger in presence of the collagen scaffolds. In all cases, MFs did not affect cell proliferation values determined by MTT assay (not shown).

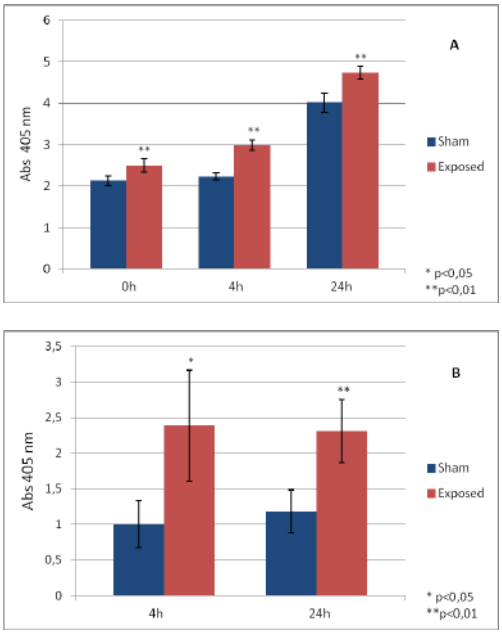

Figure 2. Alkaline phosphatase activity of SaOS-2 cells cultured in absence (A) or in presence of bone scaffolds (B) 0, 4 and 24 h after 1 h MFs exposure.

These data allow to consider MF exposure as a procedure to increase osteogenesis, as alkaline phosphatase activity is a typical marker of these processes [10]. In addition, since the higher increases of ALP activity were obtained in presence of scaffolds, MF exposure seems to be particularly effective in this condition. Therefore a perspective application of this treatment can be hypothesized to maximize bone regeneration when these biomaterials have to be used within surgery.

REFERENCES

[1] M. T. Tsai, W. J. Li, R. S. Tuan and W. H. Chang, "Modulation of osteogenesis in human mesenchymal stem cells by specific Pulsed Electromagnetic Field Stimulation," *J Orthop Res.,* vol. 27(9), pp.1169-1174, Sep. 2009.

[2] J. H. Jansen, O. P. Van Der Jagt, B. J. Punt, J. A. Verhaar, J. P. Van Leeuwen, H. Weinans and H. Jahr, "Stimulation of osteogenic differentiation in human osteoprogenitor cells by pulsed electromagnetic fields: an in vitro study," *BMC Musculoskeletal Disorders*, vol. 11, pp. 188-199, Aug. 2010.

[3] E. Saino, L. Fassina, S. Van Vlierberghe, M. A. Avanzini, P. Dubruel, G. Magenes, L. Visai and F. Benazzo, "Effects of electromagnetic stimulation on osteogenic differentiation of human mesenchymal stromal cells seeded onto gelatin cryogel," *Int J Immunopathol Pharmacol.,* vol. 24(1), pp. 1-6, Mar. 2011.

[4] F. Luo, T. Hou, Z. Zhang, Z. Xie, X. Wu and J. Xu, "Effects of Pulsed Electromagnetic Field on the osteogenic differentiation of human mesenchymal stem cells," *Orthopedics*, vol. 35(4), pp. 526-521, Apr. 2012.

[5] M. De Mattei, A. Caruso, G. C. Traina, F. Pezzetti, T. Baroni and V. Sollazzo, "Correlation between pulsed electromagnetic fields exposure time and cell proliferation increase in human osteosarcoma cell lines and human normal osteoblast cells in vitro," *Bioelectromagnetics*, vol. 20(3), pp. 177-82, 1999.

[6] N. Selvamurugan, S. Kwok, A. Vasilov, S. C. Jefcoat and N. C. Partridge, "Effects of BMP-2 and pulsed electromagnetic field (PEMF) on rat primary osteoblastic cell proliferation and gene expression," *J Orthop Res*, vol. 25(9), pp. 1213-20, Sep. 2007.

[7] L. Fassina, L. Visai, Benazzo F, L. Benedetti, A. Calligaro, M. G. De Angelis, A. Farina, V. Maliardi and G. Magenes, "Effects of electromagnetic stimulation on calcified matrix production by SAOS-2 cells over a polyurethane porous scaffold," *Tissue Eng*, vol. 12(7), pp. 1985-99, Jul. 2006.

[8] P. K. Yarlagadda, M. Chandrasekharan and J. Y. Shyan, "Recent advances and current developments in tissue scaffolding," *Biomed Mater Eng*, vol. 15(3), pp. 159-77, 2005.

[9] E. H. Groeneveld, J. P. van den Bergh, P. Holzmann, C. M. ten Bruggenkate, D. B. Tuinzing and E. H. Burger, "Mineralization processes in demineralized bone matrix grafts in human maxillary sinus floor elevations," *J Biomed Mater Res*, vol. 48(4), pp. 393-402, 1999.

[10] C. F. Martino, D. Belchenko, V. Ferguson, S. Nielsen-Preiss and H. J. Qi, "The effects of pulsed electromagnetic fields on the cellular activity of SaOS-2 cells," *Bioelectromagnetics*, vol. 29, pp. 125–132, Feb. 2008.

Exposure Of SH-SY5Y Cells To Inhomogeneous Static Magnetic Field (31.7-232.0 mT) During Cisplatin Administration

Cristian Vergallo[a], Meysam Ahmadi[b,c], Hamid Mobasheri[c,d] and Luciana Dini[§,a]
[a]*Department of Biological and Environmental Science and Technology (Di.S.Te.B.A.), University of Salento, 73100 Lecce, Italy*
[b]*Neuroscience Research Center, Institute of Neuropharmacology, Kerman University of Medical Sciences, 76175-113 Kerman, Iran*
[c]*Laboratory of Membrane Biophysics and Macromolecules, Institute of Biochemistry and Biophysics and* [d]*Biomaterials Research Center (B.R.C.), University of Tehran, 13145-1384 Tehran, Iran*
[§]*e-mail: luciana.dini@unisalento.it; phone: +390832298614; fax: +390832298937*

Summary — **The effect of Magnetic Resonance Imaging (MRI) exposure to cancer patients with CisPlatin (CP) regimen needs to be elucidated. Thus, we designed a system producing SMF induction comparable to MRI for exposure of SH-SY5Y cells treated with CP. The protective role of 31.7-232.0 mT SMF for healthy tissues in which low CP concentrations diffuse is reported.**

I. Introduction

Studies concerning the biological effects of Static Magnetic Field (SMF)-exposure highlight detrimental as well as beneficial effects [1-2]. Nevertheless, the use of permanent magnets for therapeutic purposes encouraged by basic science publications is increasing. Magnetotherapy provides a non-invasive, safe, and easy method to directly treat the site of injury, the source of pain and inflammation, and other types of disease [2-3]. Interestingly, it is recently emerging that one of the methods providing a new strategy for the effective treatment of cancer is the combinatorial effect of SMF exposure and drugs [4-5]. However, this combinatorial effect still needs an exhaustive investigation.

Cancer patients are often subjected to MRI and this happens most of the times during chemotherapeutic regimen. MRI diagnosis requires 3 different types of magnetic fields, and the B_0 component is static. Some studies have suggested that a homogenous moderate SMF of 8.8 mT produced by a solenoid can enhance the killing potency of CP on human leukemic cells K562 [4].

Taking into account what said above, the aim of the present work is the study of the possible synergism or antagonism between SMF and CP, in term of efficiency of cell death on neuroblastoma SH-SY5Y cells. The cells were simultaneously treated with 0.1 μM CP and an inhomogeneous SMF with a magnetic induction ranged between 31.7 and 232.0 mT for up to 24h.

II. Materials and Methods

SMF was produced by three magnetic parallelepipeds of NdFeB, sized 50.8 x 50.8 x 25.4 mm, coated with Ni, grade N40, Br 1260-1290 mT and supplied by Webcraft GmbH (Uster, Switzerland). These magnets were kept together by attraction in a structure made of six shelves of plexiglass plates to obtain two separate SMF exposure chambers, for the simultaneous exposure of two cell culture flasks of 25 cm^2. Magnetic field inductions were measured by using a Gaussmeter GM04 (Hirst Magnetic Instruments Ltd, Tesla House, Tregoniggie, Falmouth, Cornwall, UK), operating at the sensitivity range of 0-to more than 3T, 1 mT of resolution and ±1% of accuracy. Fig. 1 represents the exposure system and the allocation of the culture flasks.

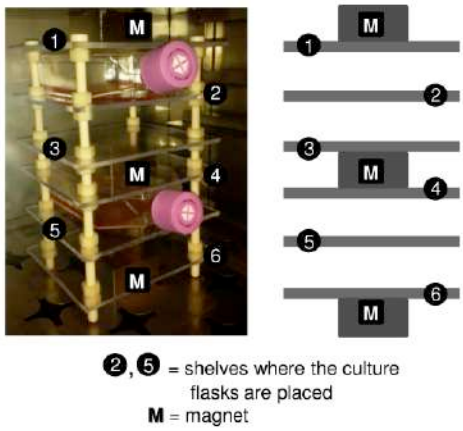

Fig. 1 Picture (left) and schematic representation (right), not in scale, showing the locations where the magnets and the culture flasks placed within the SMF exposure system.

Human adrenergic neuroblastoma cell line SH-SY5Y (10^6 cells/ml) in Dulbecco's Modified Eagles Medium, supplemented with 10% (v/v) inactivated Fetal Calf Serum, 2 mM L-glutamine, 100 IU/ml penicillin and streptomycin in a humidified atmosphere of 5% CO_2 at 37 °C were cultured. Cells underwent the following treatments: no treatment (control), CP administration (0.1, 0.5, 1 μM), SMF exposure, or SMF+CP. Cells, growing in adhesion, were exposed to an inhomogeneous SMF with a magnetic induction ranged between 31.7 and 232.0 mT. Biochemical (MTT for cell viability, NBT for ROS-generation, Western blot of Caspase-3 for apoptosis) and morphological (light and electron microscopy) investigations were done after each treatment.

ANalysis Of VAriance (ANOVA) at the 95% confidence level was performed. The error bars represent the Standard Errors (SEs) of six independent experiments each done in duplicate.

III. Results

SH-SY5Y cells were sensitive to CP whose cytotoxicity was dose-dependent (Fig. 2A). CP is an anticancer drug whose cytotoxicy is via DNA-damaging and consequent induction of apoptosis. Caspase-3 (a marker of apoptosis) was overexpressed within 2h of administration of CP (46% more than control cells) and decreased with time, in cells treated with 0.1 μM CP. Interestingly, at 2h of incubation, different concentration of CP induced different types of cell death:

with 0.1 μM CP, 75±5% cells were apoptotic and with 1 μM CP 65±5% of cells were necrotic. The production of ROS was dependent on the concentration of CP. About 23% more ROS were found in SH-SY5Y cells treated with 0.1 μM CP for 2h compared to control cells. Since the lower concentration of CP used in this work was able to induce mostly apoptosis, this concentration was chosen to investigate the effect on CP treated cells in the presence of SMF.

CP-induced toxicity was prevented by SMF in a time-dependent manner (Fig. 2B), thus suggesting that SMF is antagonist towards the CP chemotherapy efficiency. SMF exposure during CP administration extensively prevented the cell loss and the morphological alteration determined by CP, like round shape, retracted neuritis and damaged mitochondria. In addition, SMF exposure reversed the ROS generation induced by 0.1 μM CP.

At short time (2h) of simultaneous treatment with CP and SMF, the amount of Caspase-3 was only about 65% of untreated control cells.

IV. Discussion

In this study, which aimed to simulate what should happen to cancer patients under CP regimen undergoing MRI diagnostic, evidences of protection against CP toxicity by exposure to an inhomogeneous SMF (from 31.7 to 232.0 mT) of neuroblastoma SH-SY5Y cells are reported. It is worth to note that the magnetic induction has different values in various parts of the human body (in particular those that are deep inside) due to the differences of distances from the SMF source. It has been reported that SMF biological effects are not directly correlated to SMF intensity. Low induction values can be more effective than high ones [6-9].

The efficient induction of cell death caused by CP is in agreement with other reports [10] as well as the drug concentration drives the cell death types (*i.e.* apoptosis or necrosis). The decrement of the efficacy of the CP, *i.e.* Caspase-3 overexpression diminished with time, is in agreement with the fact that CP degrades with time [11]. It is most likely that apoptosis, in our system, is executed through the mitochondrial pathway, as the mitochondria damage after CP incubation strongly suggests. On the other hand, mitochondrial pathway of apoptosis seems to be the main apoptotic pathway used by SH-SY5Y cells also when treated with other anticancer drugs [12]. Contribution of ROS in the induction of apoptosis and/or cell death have to be considered, due the significant increment of ROS generation found with 0.1 μM CP for 2h, suggesting that ROS are responsible for the cell loss observed in the first 2h of treatment with CP and for the mitochondria damage. On this scenario, the biological synergic or antagonistic effects of SMF is particularly intriguing, since it is already known that the SMF can induce a dramatic modification of the cell death response when drugs are simultaneously administered [8]. Conversely to the data reported by Tenuzzo *et al.* [8], CP in presence of SMF was less effective; in fact Caspase-3 expression was 35% less than controls.

In conclusion, the overall data reported here give two contradictory indications. On one hand the data suggest that inhomogeneous SMF with a magnetic induction ranged between 31.7 and 232.0 mT protects the cells against CP cytotoxicity, at least for up to 24h. However, this view on perspective of cancer patients undergoing chemotherapy is certainly undesired; indeed SMF exposure could compromise the success of chemotherapy of CP-treated patients, because it could reduce the effectiveness of the drug by its anti-apoptotic action. On the other hand, SMF could be exploited to counteract the cytotoxic effects due to CP, which could diffuse at low concentrations in healthy tissues of patients. It should be further investigated if this beneficial effects of SMF, observed in our *in vitro* study, could be translated into evidence-based medical therapy options available to clinicians to prevent the side effects of the CP-based chemotherapy.

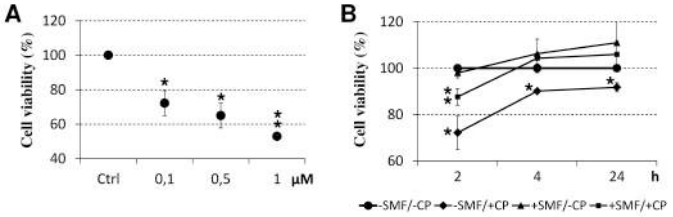

Fig. 2 A: viability (MTT assay) of SH-SY5Y cells treated with different concentrations of CisPlatin (CP) (0.1, 0.5 or 1 μM) for 2h. B: time-course of viability (MTT assay) of 0.1 μM CP-treated and/or Static Magnetic Field (SMF)-exposed cells for 2, 4 or 24h. Values are reported as percentage of the control untreated cells considered as 100%. Single star indicates values significantly different from the respective untreated control cells. Two stars indicates value significantly different either from 0.1 μM CP-treated that from untreated control cells.

References

[1] A. Heinrich, A. Szostek, F. Nees, P. Meyer, W. Semmler, and H. Flor, "Effects of Static Magnetic Fields on Cognition, Vital Signs, and Sensory Perception: A Meta-analysis" *J. Magn. Reson. Imaging*, vol. 34, pp. 758–763, 2011.

[2] C. Vergallo, L. Dini, Z. Szamosvölgyi, B.A. Tenuzzo, E. Carata, E. Panzarini, and J.F. László, "In Vitro Analysis of the Anti-Inflammatory Effect of Inhomogeneous Static Magnetic Field-Exposure on Human Macrophages and Lymphocytes" *PLoS ONE*, vol. 8, e72374, 2013.

[3] M.S. Markov, "Magnetic field therapy: a review" *Electromagn. Biol. Med.*, vol. 26, pp. 1–23, 2007.

[4] Y. Liu, H. Qi, R.G. Sun, and W.F. Chen, "An investigation into the combined effect of static magnetic fields and different anticancer drugs on K562 cell membranes" *Tumori*, vol. 97, pp. 386-392, 2011.

[5] R.G. Sun, W.F. Chen, H. Qi, K. Zhang, T. Bu, Y. Liu, and S.R. Wang, "Biologic effects of SMF and paclitaxel on K562 human leukemia cells" *Gen. Physiol. Biophys.*, vol. 31, pp. 1-10, 2012.

[6] A. Chionna, B. Tenuzzo, E. Panzarini, M. Dwikat, L. Abbro, and L. Dini, "Time dependent modifications of Hep G2 cells during exposure to static magnetic fields" *Bioelectromagnetics*, vol. 26, pp. 275–286, 2005.

[7] L. Dini and L. Abbro, "Bioeffects of moderate-intensity static magnetic fields on cell cultures" *Micron*, vol. 6, pp. 195–217, 2005.

[8] B. Tenuzzo, A. Chionna, E. Panzarini, R. Lanubile, P. Tarantino, B. Di Jeso, M. Dwikat, and L. Dini, "Biological effects of 6 mT static magnetic fields: a comparative study in different cell types" *Bioelectromagnetics*, vol. 27, pp. 560-577, 2006.

[9] L. Dini and C. Vergallo, Chapter 15th "Environmental factors affecting phagocytosis of dying cells: smoking and static magnetic fields". Title of the volume: "Phagocytosis of dying cells: from molecular mechanisms to human diseases". Volume editors: Dmitri V. Krysko and Peter Vandenabeele. *Springer Science+Business Media B.V. 2009*, Belgium, pp. 409-438, 2009.

[10] V.M. Gonzalez, M.A. Fuertes, C. Alonso, and J.M. Perez, "Is cisplatin-induced cell death always produced by apoptosis?" *Mol. Pharmacol.*, vol. 59, pp. 657–663, 2001.

[11] R.F. Greene, D.C. Chatterji, P.K. Hiranaka, and J.F. Gallelli, "Stability of cisplatin in aqueous solution" *Am. J. Hosp. Pharm.*, vol. 36, pp. 38-43, 1979.

[12] A. Marcuzzi, P.M. Tricarico, E. Piscianz, G. Kleiner, L. Vecchi Brumatti, and S. Crovella, "Lovastatin induces apoptosis through the mitochondrial pathway in an undifferentiated SH-SY5Y neuroblastoma cell line" *Cell Death Dis.*, vol. 4, e585, 2013.

Human Fibroblasts Exposed to THz Radiation: Study of Genotoxic Effects by Micronucleus Assay

A. Sgura[#], E. Coluzzi[#], C. Cicia[#], A. De Amicis*, S. De Sanctis*, S. Di Cristofaro*, V. Franchini*, E. Regalbuto*, A. Doria°, E. Giovenale°, R. Bei[+], M. Fantini[+], M. Benvenuto[+], L. Masuelli[§], F. Lista*, G.P. Gallerano°

[#]*University "Roma Tre" Department of Science – Viale G. Marconi 446, 00146 Rome – Italy*
**Army Medical and Veterinary Research Center, Rome – Italy*
°ENEA - Radiation Sources Laboratory, Frascati Research Center – Italy
[+]*University of Rome "Tor Vergata" - Department of Clinical Sciences and Translational Medicine – Rome, Italy*
[§]*University of Rome "Sapienza" - Department of Experimental Medicine - Rome, Italy*

Summary

Terahertz (THz) radiation has been increasingly used in a variety of applications. However, few data are available on the biological effects of this type of electromagnetic radiation. The aim of our study is to evaluate genotoxic effects in human fibroblasts exposed to low frequency THz using the micronucleus assay. We describe the irradiation set-up and report preliminary results.

Introduction

In recent years, Terahertz (THz) radiation has aroused a growing interest in medical, security and military applications. However, the biological effects of this type of non-ionizing radiation are still scarcely investigated. Human leucocytes and skin fibroblasts were mainly used as cellular models in proactive studies on this topic [1, 2]. Potential DNA damage induced by THz in vitro irradiation was assessed using the comet assay and micronucleus test. The Cytokinesis-Block Micronucleus (CBMN) assay, which consists in counting the micronuclei (MN) in binucleated cells (BN cells), is a feasible and rapid method to assess genotoxic damage induced by physical and chemical agents [3, 4]. The data reported in the literature on biological damage associated to THz exposure are quite contradictory. Hintzsche et al., 2012 showed no statistically significant induction of DNA strand breaks, investigated by Comet assay in two different types of skin cells exposed to THz radiation [5]. The micronucleus frequency was also not affected by the terahertz exposure in both cell types, confirming the results of other studies which found no increase in micronucleus frequency associated to terahertz radiation [6]. In contrast to this, some authors suggested that THz radiation exposure could result in mitotic disturbance, giving rise to aneuploidy in daughter cells [7; 8]. In this study we investigated the genotoxic effects of in vitro Terahertz exposure in human fetal fibroblasts using CBMN assay. The exposure was performed in the frequency range between 100 and 150 Ghz.

Material and methods

Exposure set-up

In vitro exposure of human fibroblasts HFFF2 was performed in a wide band between 100 and 150 GHz using the ENEA Compact Free Electron Laser (FEL). Due to the peculiar characteristics of the electron accelerator driving the FEL, the radiation pulse is composed by a "train" of micropulses, each 50 ps long, with 330 ps spacing between adjacent micropulses. This temporal structure of the emitted radiation allows the investigation of the effects of high peak power, while maintaining a low average power, typically few mW, incident on the sample, thus avoiding heating effects. A specific THz Delivery System (TDS) was designed and built providing the necessary expansion of the THz beam needed to match the area of the 5 cm diameter Petri dishes used in the experiments.

Cytokinesis-block micronucleus assay.

Human primary fibroblasts (HFFF2) were seeded on petri dish 24 hrs before THz exposure. Binucleated cells (BN) were obtained adding cytocalasin-B (Sigma Aldrich, St. Louis, USA) at a final concentration of 3µg/ml 24 hrs before fixation [9]. Cell cultures were fixed in freshly Carnoy modified solution (5:1 v/v methanol/acetic acid) and dyed with 4,6-diamodino-2 phenylindole (DAPI, sigma Aldrich, St. Louis, USA) in Vectashield (Vector Laboratories, Burlingame, CA). Bi-nucleated cells were scored as previously described by [4]. Cells were considered BN when the two nuclei were situated in the same cytoplasm, have more or less the same size, staining pattern and intensity pattern.

The scoring of micronuclei (MN), considered morphologically identical to a nuclei but smaller, takes into account only MN non-refractive, not linked or connected to the main nuclei and with the same staining intensity as the main nuclei or occasionally more intense [4].

Results and discussion

Results obtained from MN analysis are shown in Fig. 1. We can observe a statistically significant MN induction in irradiated samples compared to the untreated one. These preliminary results indicate an increase of DNA damage after THz exposure.

It will be interesting to perform further analysis in order to confirm this data and to better understand the origin of these MN. In fact, MN can arise from acentric fragments that fail to be incorporated into the daughter nuclei during cell division or from entire chromosomes. The latter could result from mitotic spindle alteration at mitosis or from complex chromosomal configurations that pose problems during anaphase. Thus, formation of micronuclei can be induced by both clastogenic and aneuploidy-inducing agents. The identification of kinetochores in MN by antibody staining [10]

will make possible to identify MN originating from chromosomal aberrations or chromosome loss.

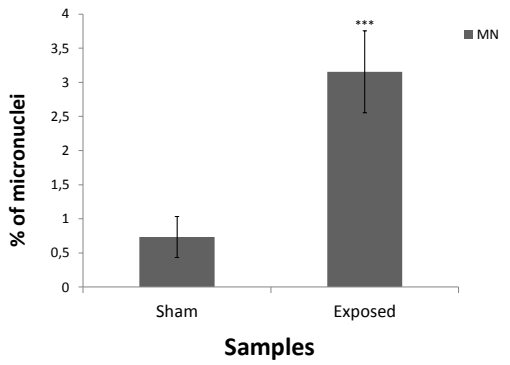

Fig.1. Percentage of MN in exposed and untreated samples. The frequencies of MN were obtained on 1000 bi-nucleated cells from two independent experiments. The statistical test used for the analysis of MN was the binomial probability test. Significance was accepted for value $p< 0.05$. ***$p<0.0001$

References

[1] M. R. Scarfì, M. Romanò, R. Di Pietro, O. Zeni, A. Doria, G. P. Gallerano, E. Giovenale, G. Messina, A. Lai, G. Campurra, D. Coniglio and M. D'Arienzo, "THz Exposure of Whole Blood for the Study of Biological Effects on Human Lymphocytes", *J Biol Phys*., vol. 29, pp 171-176, 2003.

[2] A. Doria, G. P. Gallerano, E. Giovenale, G. Messina and I. Spassovsky, "Enhanced coherent emission of terahertz radiation by energy-phase correlation in a bunched electron beam", *Phys Rev Lett.*, vol. 93, 2004.

[3] W. U. Müller and C. Streffer, "Micronucleus assays" In: Obe G (Ed.) *Advances in mutagenesis research, Springer-Verlag, Berlin*, pp. 1-134. 1994

[4] M. Fenech, "The in vitro micronucleus technique", *Mutat Res*, vol. 455 pp 81-95, 2000.

[5] H. Hintzsche, C. Jastrow, T. Kleine-Ostmann, U. Kärst, T. Schrader and H. Stopper, "Terahertz electromagnetic fields (0.106 THz) do not induce manifest genomic damage in vitro", *PLoS One*, vol. 7, 2012.

[6] O. Zeni, G. P. Gallerano, A. Perrotta, M. Romanò, A. Sannino, M. Sarti, M. D'Arienzo, A. Doria, E. Giovenale, A. Lai, G. Messina and M. R. Scarfì, "Cytogenetic observations in human peripheral blood leukocytes following in vitro exposure to THz radiation: a pilot study"' *Health Phys.*, vol. 92, pp 349-357, 2007.

[7] A. Korenstein-Ilan, A. Barbul, P. Hasin, A. Eliran, A. Gover and R. Korenstein, "Terahertz radiation increases genomic instability in human lymphocytes", *Radiat Res*, vol. 170, pp 224-234, 2008.

[8] H. Hintzsche, C. Jastrow, T. Kleine-Ostmann, H. Stopper, E. Schmid and T. Schrader, "Terahertz radiation induces spindle disturbances in human-hamster hybrid cells", *Radiat Res*, vol. 175, pp 569-574, 2011.

[9] M. Kirsch-Volders, I. Tallon, C. Tanzarella, A. Sgura, T. Hermine, E. M. Parry and J. M. Parry, "Mitotic non-disjunction as a mechanism for in vitro aneuploidy induction by X-rays in primary human cells", *Mutagenesis*, vol 11, pp 307-313, 1996.

[10] A. Sgura, A. Antoccia, R. Cherubini, M. Dalla Vecchia, P. Tiveron, F. Degrassi and C. Tanzarella, "Micronuclei, CREST-positive micronuclei and cell inactivation induced in Chinese hamster cells by radiation with different quality" *Int J Radiat Biol.*, vol. 76, pp 367-374, 2000.

Exposure by WLAN in an Indoor Environment

Luciano MONDINI*, Carlo SBRANA**, Fulvio ARREGHINI**

**Health Physics Department, Azienda Sanitaria Locale n.5 – East Hospital, Via del Forno, n.4 19100 - La Spezia, e-mail : lucimond1959@libero.it*

***" - Italian Navy-Electronic and Telecommunication Institute "G.Vallauri"-Viale Italia, n.72 , 57100- Livorno,,e-mail: fulvio.arreghini@gmail.com*

Abstract - investigated topics of this study are: (I) Assessment of the Electric field in a home scenario with particular regard to an infant bedroom (II)verification of the compliance to Italian regulatory limits concerning population exposure to EM fields (III) Comparison the Electric field strength measured with values expected by a single commercial WLAN transmitter (100mW – 2400 Mhz) (IV)Determination of the safety distance at where Electric field strength reach the regulatory limit value (zoning – CENELEC EN 50499).

Key words: E-field exposure assessment, finite- difference methods; environmental safety

I. INTRODUCTION

Today different kind of wireless communication systems are present in almost every home. As a result of this phenomena, the assessment of the exposure level in typical home environment has to take into account not only the devices located within the single house or flat, but also the contribution to these field caused by emitters located in the neighborhood: though the emitted field from these devices is attenuated by the walls, their number can be significantly high, so that the sum of all the generated field is to be taken into account.This contribution presents an assessment of the human exposure to electromagnetic fields caused by home wireless communication systems. For this purpose we investigated the emissions of Wireless LAN (IEEE 802.11) devices in a typical two-floors home environment. First, a simulation of the real scenario was created, in order to derive the theoretical distribution and strengths of the EM fields. As a second step, a measurement in controlled environment (anechoic chamber) was performed to calibrate the instrumentation and to obtain a reference situation. Finally, the measurements were carried out in the real scenario. The measurement outcomes were then compared with the limits imposed by Italian regulations on EM protection(DPCM n. 199/2003).

II. MATERIALS, METHODS, RESULTS

The investigated scenario takes into consideration an indoor environment (i.e. a room) surrounded by a dense distribution WLAN Emitters. Emitters positions, frequencies and power are not known a priori. A children bedroom, is taken into consideration as the most critical measurement point: in this area a child is supposed

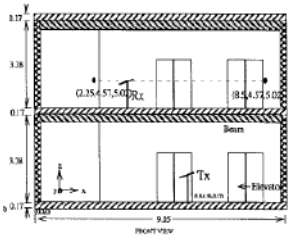

Figure 1: measurement scenario model

to sleep all night long , so we have to take into account the most severe Italian regulatory limits stating that the E field strength shall not exceed 6 V/m. The bedroom under investigation is modeled using a ray-tracing method for indoor propagation[3]. Two different floors of 5m x 9m x 3.2m are shown in the map(Figure 1). At first floor, the receiving dipole antenna (Rx) was moved along a straight path directly above the ground floor dipole antenna (TX), transmitting at frequencies of 1800 MHz with horizontal polarization.The comparison between simulated attenuation and measured one at the minimum (4m) distance between Rx and TX antennas, taking into account the shielding of 17cm thick floor, are shown in Figure 2.

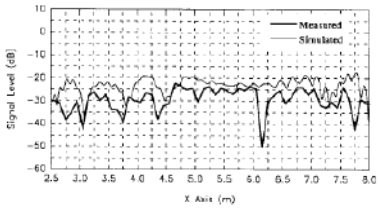

Figure 2: comparison between calculated and measured attenuation

Using an hyperlog instead of a dipole antenna, next step was characterize the SWR. Rohde & Schwartz FS4H-NA were used to obtain the hyperlog 2-3 GHz SWR shown in Figure 3.

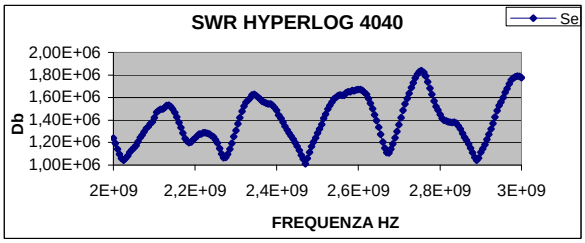

Figure 3: SWR characterization

To define the expected Electric field amplitude as a function of distance from the single WLAN emitter, measurements of the maximum incident electric field strength in an anechoic chamber (at Electronic and Telecommunication Institute "G.Vallauri"- Livorno) were carried out. The WLAN emitter was modeled with a calibrated Double Ridge Horn Transmitter (100mW @ 2450 MHz)[1], towards to an HyperLOG 4040 AARONIA Receiving antenna, located respectively 2, 3 and 4 m distance. Output of transmitter antennas was measured by a Rohde & Schwartz 828-3818-02 Power Sensor. Knowing the DRG Horn output P(W) and linear Gain G, at d(m) distance in far field expected E (V/m) is:

$$E = \frac{\sqrt{(30PG)}}{d}$$

Measures were made simultaneusly with calibrated PMM 8053A sensor and HyperLog 4040 antenna. Comparing the expected and measured E values we obtain a good agreement among the E values at different Tx-Rx distances (Table 1) .

DRG Horn P (W)	Freq Rx	Tx-Rx d (m)	Expected E (V/m)	PMM 8053A E (V/m)	Hyperlog 4040 E (V/m)
0,1	2450	2	2,42761958	3	2,107
0,1	2450	3	1,618413054	1,67	1,634
0,1	2450	4	1,21380979	1,26	1,398

Table 1: E values versus distance

The same measures expected in the environmental scenario and simulated[3] are obtained in the anechoic chamber between antennas RX-TX respectively at 4m distance, interposing a 12 cm thick wall located at 10cm distance from the receiving antennas (Figure 4).

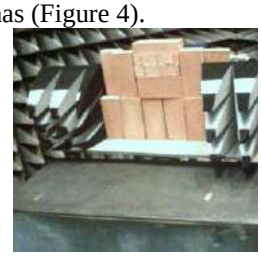

Figure 4: wall built during measurement process

Despite of different conditions for frequency (1,8 GHz vs. 2,45 GHz) and wall thickness (17cm vs. 12 cm) differences, measured dB attenuation confirms what expected [3](Table 3)

	d(m) Tx-Rx	Floor (m)	dB Simul	dB Meas	dB Mean
Simulated Ray Tracing Method	4	0,17	-22	-25	**-23,5**
Measured by PMM 8053A	4	0,12	4,855239161	0,35	**-22,84**
Measured by Hyperlog 4040	4	0,12	4,855239161	0,353	**-22,77**

Table 2: measurement with wall

Indoor measurements were performed during daytime when the maximum traffic load in the network is expected. Measures are made respectively at 10cm and 40 cm distance over the floor, under the children bed. For all measurements of E the former AARONIA SPECTRAN HF 4040 with EMC directional Antenna HyperLOG (400Mhz – 4 GHz) and real time handheld Spectrum Analyzer Software running on notebook were used, in order to obtain results comparable with the DPCM n.199/2003 limits, in which 6-min average of field quantities are of interest[1].All the dBm Hyperlog measure are recorded in logger way, sweeping the 2,4 – 2,5 GHz band during the measure (Table 4) and corrected by the SWR curve to obtain the MAX E value. (in graph –measure at 10cm from the floor).

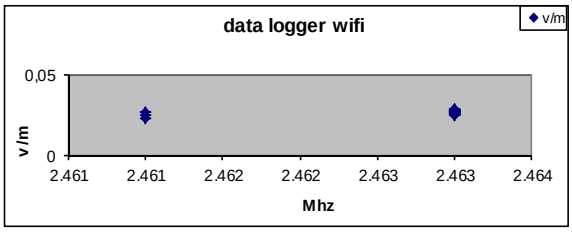

Figure 5: E values versus frequency

Comparison of the measures made with Rx antenna at 10cm distance from shield, demonstrates a floor attenuation two times the wall attenuation measured in the anechoic chamber , in agree with a major floor thick.(Table 5)

Table 3: measurements comparison

	d(m) Tx-Rx	Expected E (V/m) 4m Tx	E(V/m)wall	Floor (m)	PL(R0)	PL(dB)	WAF (dB)
Measured by PMM 8053A	4	1,21380979	0,35	0,12	**-12,041**	**-22,84285166**	**-10,80165183**
Anecoic chamber Hyperlog	4	1,21380979	0,353	0,12	**-12,041**	**-22,76871844**	**-10,72751861**
Environment Hyperlog	4	1,21380979	0,028	?	**-12,041**	**-32,73985209**	**-20,69865227**

The propagation path is then observed during the measurements, depending of the distance and mutual positions of the transmitting and the receiving antennas.

The exponential decrease of E amplitude versus distance derived from literature[2] has then been verified experimentally.(Figure 6)

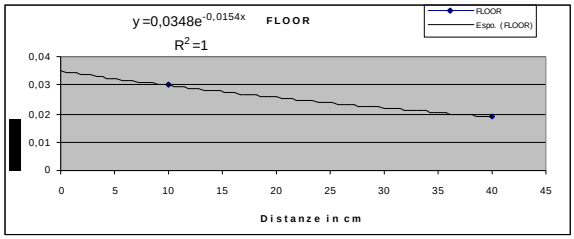

Figure 6: attenuation model

The exposure indicators for population in the radio frequency fields of the considered applications, is below 1% of the reference Electric field limit imposed by regulations. (see table)

Distanza cm		E (V/m)
0		
10		0,029875307
20		
30		
40		0,018829641
Liv. Attenzione		6
% Max/liv.att.		0,498%
Modello	FLOOR	
Estensione della Zona 1 (altezza in cm dal pavimento)	6,00	-334,41

Table 4: Exposure indicators

III. CONCLUSIONS

Results demonstrate that even under non usual conditions, the exposure indicators for population in the radio frequency fields of the considered applications, is below 1% of the reference Electric field limit imposed by regulations. Anyway we observed that the exposure caused by an emitter located in a surrounding room (and even in another floor) is similar to the one caused by an emitter located inside the room where measures are performed. The exposure determination then need to take into account all the electromagnetic scenario and the effects of obstacles and shielding structures.

IV. ACKNOWLEDGMENT

The autors would like to acknowledge the valuable support from Michelino MONDINI .

REFERENCES

[1] Schmid G, Lager D, Preiner P, U¨ berbacher R, Cecil S. 2007. Exposure caused by wireless technologies used for shortrange indoor communication in homes and offices. Radiat Prot Dosim 124(1):58–62.

[2] Martinez M , Martin A, Sanchis A, Villar R, 2009. FDTD Assessment of Human Exposure to Electromagnetic Fields From WiFi and Bluetooth Devices in Some Operating Situations. Bioelectromagnetics 30: 142-151

[3] Chang-Fa Yang, Boau-Cheng , Chuen-Jyi Ko, 1998. A Ray-Tracing Method for Modelling Indoor Wave Propagation and Penetration.IEEE Transactions on antennas and propagation, Vol.46 No.6 : 907-919

Human exposure evaluation to mobile phone electromagnetic emissions

Giovanni d'Amore[#], Laura Anglesio[#], Alberto Benedetto[#], Mauro Mantovan[#], Massimiliano Polesel[#]

[#]*Radiation Department, Regional Environmental Protection Agency of Piemonte (ARPA Piemonte) , via Jervis 30 Ivrea (TO), g.damore@arpa.piemonte.it*

***Abstract* — In this study was investigated the transmitted (Tx) power of mobile phones for different usage modes and in different conditions of environmental signal reception. Tx power was measured by an experimental system set-up for this investigation. The variation of mobile phone exposure for the operation with 2G or 3G network technologies and for different levels of environmental signals was analyzed.**

I. INTRODUCTION

Output power of the mobile phones is an important factor for exposure assessment of electromagnetic fields emitted by these devices. So the characterization of time variation of output power is of interest to evaluate the differences in level of exposure to mobile phones and to estimate the people exposure during real use in operating networks [1,2,3]. Time variation of phone output power is due to power control technologies which regulate transmitted power depending on the received signal strength (Adaptive Power Control – APC). Previous works evaluated output power via software by network analysis tool [4,5]. In this study, measurements of transmitted power were made for three models of smart phone operating both in GSM and in UMTS networks. To verify the variability of transmitted power with network technology, the smart phones were forced to operate with only one technology. Further tests were carried out considering the two different usage modes: voice call and data transmission.

Output power was determined by on site measurements in seven areas with different reception quality and electric field exposure levels.

II. EXPERIMENTAL SET UP

The instrumental chain for radiofrequency power emitted from mobile phones is shown in figure 1.

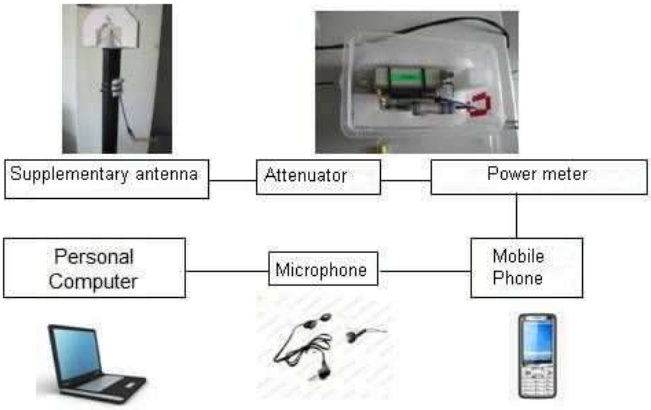

Fig. 1 Measurement system set up for output power of mobile phones

A supplementary antenna outside the mobile phone was used because the signal detection at the feeding connector of inner antenna was not possible. A variable attenuator was added into the system before the signal entered the outside antenna and the attenuation value was fixed so that quality reception was comparable with that of inner antenna (about 20 dB). RF output power was measured by power sensor R&S mod. FSH-Z1 with a frequency range 10 MHz - 8GHz and a dynamic range 200 pW – 200 mW. Power sensor, connected to mobile phone by a directional coupler, was remotely controlled by a self made application based on LabView. Power measurements were acquired with a time step of 30 msec for determining average and maximum exposure during mobile phone usage. Usage mode of phone was standardized by reproducing a typical registered voice call and by downloading the same video during tests on data mode.

Environmental electric field levels were measured for relating exposure levels and quality reception with phone transmitted power. These measurements were carried out by spectrum analyzer Narda mod. SRM3000 connected to a triaxial antenna. By this instrumental chain, the Broadcast Control Channel (BCCH) signal level was measured in frequency domain, for GSM network, and Common Pilot Channel (CPICH) power was measured in code domain, for UMTS signal [6]. BCCH and CPCIH level do not depend on the traffic load and they can be good indicators of reception level for GSM and UMTS signals in the investigated area.

Tests were made on three different models of smart phones.

III. RESULTS AND DISCUSSION

An example of mobile phone transmitted power measured for the three considered usage mode is shown in figure 2.

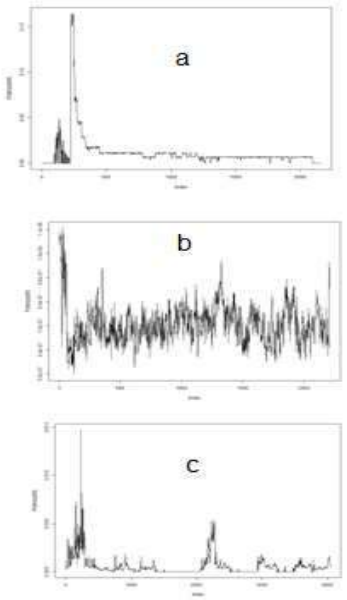

Fig. 2 Example of measured transmitted power of mobile phone for three usage mode: a) voice call with GSM network, b) voice call with UMTS network, c) data mode with UMTS network.

Figure 2a shows the peak level due to setting initial uplink transmission power when mobile phone is accessing to GSM network. Graph in figure 2b shows a typical noise like transmitted signal due to the codes used in UMTS technology which have a pseudo random bit sequence. In figure 2c the different peak levels are representative of the packet mode communication.

Average output power measurement results as a function of environmental electric field (BCCH and CPICH levels) are shown in figure 3 for one of the tested smart phones.

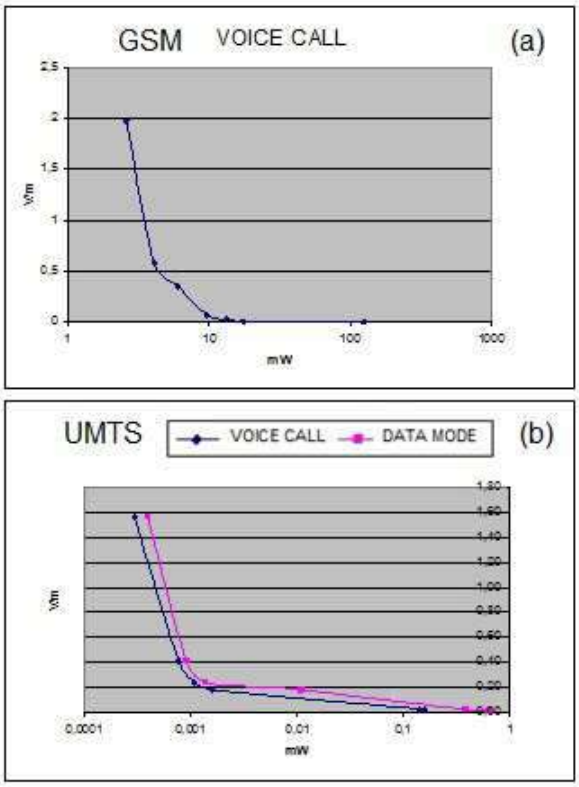

Fig. 3 Average output power versus environmental electric field for one of the tested mobile phones: a) GSM network; b) UMTS network for voice call and data transmission usage mode

Measured transmitted power changed as a function of electric field reception level. For GSM voice call the average transmitted power varies from 2 mW, in areas with electric field strength of about 2 V/m, to levels higher than 100 mW, in areas with electric field strength of about 0.001 V/m. So the reduction in electric field level of a factor of 2000 corresponds to an increasing of transmitted power of a factor of about 60. Similarly, we observed the transmitted power increasing with the reduction of reception level for UMTS voice call and data transmission mode. The average transmitted power for UMTS voice call varies from 0.4 µW to some mW passing from areas with electric field of about 1 V/m to areas with lower levels (0.01 V/m).

The above reported results indicate also that mobile phone average output power for UMTS voice call is very lower than for GSM voice call in all investigated environments. The difference between average output powers is of a factor of 15 in environments with low reception level (100 mW for GSM and some mW for UMTS). This difference raises to a factor of 5000 in environments with high reception levels, where average output power passing from 0.4 µW for UMTS network to 2 mW for GSM network.

IV. CONCLUSIONS

In this study the real transmitted power for GSM and UMTS services was measured in different configurations. Variation of average output power of mobile phones was quantified with relation to environmental reception level.

Measurement results indicate that exposure level to GSM mobile phone in outdoor areas with higher environmental electric field strengths and a good reception quality is 60 times lower than in indoor situation with bad signal reception. This variability in exposure levels is much higher for UMTS voice call usage reaching a factor of about 2000. In the investigated areas, exposure levels due to UMTS voice calls resulted from 15 times to 5000 times lower than those due to GSM voice calls.

Further studies will be necessary to compare head exposure to mobile phones with whole body exposure to environmental radiofrequency fields from base stations.

AKNOWLEDGMENT

This research was funded by the Regional Committee for Communication in Piedmont (CoReCom Piemonte).

Mobile phones for tests, coaxial cable for their connection and supplementary antenna were kindly provided by laboratory of Telecom Italia (TiLab) in Turin.

REFERENCES

[1] Vrijheid M., Mann S., Vecchia P., Wiart J. et al. (2009) Determinants of mobile phone output power in a multinational study: implications for exposure assessment. Occupational and Environmental Medicine. Vol. 66, n. 10, pp 664-671

[2] Ardoino L., Barbieri E. and Vecchia P. (2004) Determinants of exposure to electromagnetic fields from mobile phones. Radiation Protection Dosimetry. 111, pp- 403-406

[3] Balzano Q. (1999) Exposure metrics for RF epidemiology: cellular phone handsets. Radiation Protection Dosimetry 83, pp 165-169

[4] Wiart J., Dale C., Bosisio AD, et al. (2000) Analysis of the influence f the power control and discontinuation tranmission on RF exposure with GSM mobile phone. IEEE Transactions on Electromagnetic Compatibility. 42, pp 376-385

[5] Gati AG, Hadjem A., Wong MF and Wiart J. (2009) Exposure induced by WCDMA mobile phones in operating network. IEEE Transactions on Wireless Communication. Vol. 8, n. 12, pp. 5723-5727

[6] S. Trinchero, A. Benedetto, L. Anglesio, G. d'Amore and D. Trinchero, "Exposure Measuring Techniques for Wide Band Mobile Radiocommunication", Radiation Protection Dosimetry, Special Issue, vol. 111, n° 4, pp.429-434,2004

Indoor levels of ELF magnetic fields in buildings with built-in transformers

Susanna Lagorio[*], Leeka Kheifets[+]

[*] *National Centre for Epidemiology Surveillance and Health Promotion, National Institute of Health, Viale Regina Elena, 299 00161 Rome (Italy), susanna.lagorio@iss.it;*

[+] *Department of Epidemiology, UCLA Fielding School of Public Health, 650 Charles E. Young Drive South CA 90095-1772 Los Angeles, CA (USA), kheifets@ucla.edu*

Abstract— **In the framework of the feasibility of an international study on ELF magnetic fields and leukemia in children living in buildings with built-in transformers (TransExpo), we have assessed whether an a priori classification of the apartments, based on its distance from the transformer room, is predictive of the indoor magnetic field level. We summarize herein the preliminary results of the exposure validation study performed in Italy.**

I. Introduction

In 2002 the International Agency for Research on Cancer (IARC) classified extremely-low-frequency magnetic fields (ELF-MF) as ‘‘possibly carcinogenic in humans’’ (group 2B), based on limited evidence in humans (in relation to childhood leukemia only) and inadequate evidence in experimental animals [1].

The IARC evaluation was driven by an increased risk of leukemia with daily average exposure to ELF-MF above 0.3 or 0.4 μT observed in two partially overlapping pooled analyses of about a dozen epidemiological studies published by the turn of the century [2-3].

A pooled analysis of 7 new studies broadly replicated earlier findings [4].

Unfortunately, the new studies share the methodological shortcomings of the previous ones. Therefore, due to lack of support from experimental studies and plausible mechanism, bias and/or uncontrolled confounding remain plausible alternative (non-causal) explanations of the epidemiological findings [5-7].

To reduce the scientific uncertainty new approaches are required; only studies designed to minimize biases from different sources while maximizing the ability to detect an association, should one exist, could provide relevant new information [8]. One such study is “TransExpo”, an international study of childhood leukemia among children living in apartment buildings with built-in electrical transformers, whose feasibility is currently being evaluated or piloted in several countries, including Italy [9-10].

II. Main features of the TransExpo study

People living in buildings with transformers form a study population which includes individuals exposed to different levels of ELF-MF (well over the background in apartments adjacent to the transformer), but likely more homogeneous in terms of socio-economic status and other environmental exposures than persons not living in such buildings.

The assessment of exposure to ELF-MF will be based on the relative location of the transformers and residences within the building, without contact with the study participants, and blind to the children’s health status.

The basic assumption in the main epidemiologic study is that residents of apartments in close proximity (immediately above or adjacent) to transformer rooms are exposed to magnetic field exposure levels significantly higher than average residential exposure levels in other apartments in the same buildings and that these exposures can be predicted without access to the residence.

We report on methods and preliminary results of a measurement survey carried out in Italy, aimed to assess the reliability of an *a priori* exposure classification, based on the distance of the apartments from the transformer room.

III. Methods

The measurement protocol called for a series of measurements of magnetic field level in a sample of buildings with built-in transformers.

In each of these building, 3 to 5 apartments had to be selected, at least one for each of the following categories:

- Directly above the transformer room (type 1) or sharing an edge with it (type 2);
- On the same floor of type 1 apartments but not contiguous to the transformer room (type 3) or one floor above type 1 apartments (type 4);
- Other floors and locations not considered above (type 5).

In each apartment the following series of measurements were to be made, using an EMDEX II or an EMDEX Lite magnetic field meter (full frequency range 40-800 Hz including harmonics):

- a spot measurement at the front door;
- a series of spot magnetic field measurements in every commonly occupied room of the residence (one at the center of the room and four at halfway between the center and the corners of the room);
- an additional spot measurement at the center of each bed in each bedroom;
- a 24 hour recording of the magnetic field level in the bedroom (preferably that occupied by the youngest resident), placing an EMDEX meter (sampling frequency = 5 seconds) at a convenient, unobtrusive location.

Concurrent in time with the 24 h measurements in the various apartments from any particular building, a 24 hour recording of the magnetic field level in the transformer room of each building would also be performed, placing an EMDEX (II or Lite) meter in proximity to the emergence of the secondary cabling.

The spatial coordinates (north, east, quote) of the locations of the frontdoor and 24 h measurements (in the bedrooms and

the transformer rooms), with a common origin, had to be recorded.

IV. PRELIMINARY RESULTS

The survey was carried out in Milan, in cooperation with technicians of the local power distribution company (A2A Reti Elettriche), between December 2012 and February 2014.

A sample of 26 buildings was extracted from the A2A database of MV-LV transformers in Milan (5,466 substations as of September 2012).

More than half of the sampled buildings, however, had to be excluded for various reasons [the transformer room was located in the courtyard, not inside the residential building (#3); the apartments adjoining the transformer room were not for residential use (#4); tenants were not identifiable from intercom or mailboxes (#2); repeated unsuccessful attempt to approach occupants of apartments adjoining the transformer rooms (#4); occupants of apartments adjoining the transformer rooms refused to participate in the survey (#3)], leaving 10 buildings (38%) suitable for inclusion in the study.

Out of 40 residents in the 10 eligible buildings who could be identified, 35 were contacted and invited to participate in the study (88%), 29 agree to take part in the measurement survey (83%) and 26 were at home on the appointment date (74%). Participation rates were higher among occupants of apartments adjoining the transformer room (10/10; 100%), than among persons living in apartments located further away (16/25; 64%).

The average level of magnetic field from the 24 h bedroom recording was substantially higher in apartments adjoining the transformers rooms compared to all other apartment types (Table I), while our *a priori* medium and low categories of potential exposure showed similar average levels of ELF-MF (Figure I).

TABLE I

AVERAGE LEVELS OF ELF-MF (μT) FROM 24 H BEDROOM MEASUREMENTS IN APARTMENTS FROM BUILDINGS WITH BUILT-IN TRANSFORMER, BY *A PRIORI* CATEGORIES OF EXPOSURE POTENTIAL

Potential exposure*	N°	Mean (SD)	IQR	p§
High	12	0.45 (0.24)	0.24-0.58	<0.0001
Low	14	0.09 (0.06)	0.04-0.13	

*High = type 1 or 2 apartments; Low= type 3, 4, or 5 apartments.
§Kruskall-Wallis test on the group arithmetic means.

FIGURE I

AVERAGE LEVELS OF ELF-MF (μT) FROM 24 H BEDROOM MEASUREMENTS IN APARTMENTS FROM BUILDINGS WITH BUILT-IN TRANSFORMER, BY *A PRIORI* CATEGORIES OF EXPOSURE POTENTIAL (HIGH, MEDIUM, LOW)

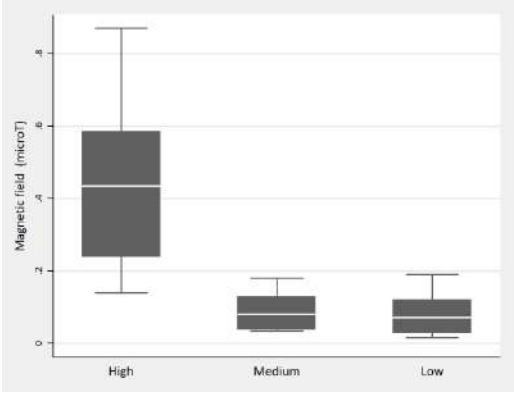

V. CONCLUSIONS

The preliminary results of the Italian pilot study, in line with findings from other countries participating in the TransExpo feasibility study [11-16], are encouraging and confirm the assumption that residents in apartments in close proximity to transformers are exposed to magnetic fields significantly higher than in other apartments in the same building.

REFERENCES

[1] IARC (International Agency for Research on Cancer), *Non-Ionizing Radiation, Part 1: Static and Extremely Low-Frequency (ELF) Electric and Magnetic Fields*, IARC Monographs on the Evaluation of Carcinogenic Risks to Humans: vol. 80, Ed. Lyon, France: IARC Press, 2002.

[2] A. Ahlbom et al., "A Pooled Analysis of Magnetic Fields and Childhood Leukemia", Br J Cancer, vol. 83, pp. 692-698, 2000.

[3] S. Greenland et al., "A Pooled Analysis of Magnetic Fields, Wire Codes, and Childhood Leukemia", Epidemiology, vol. 11, pp. 624–634, 2000.

[4] L. Kheifets et al., "Pooled Analysis of Recent Studies on Magnetic Fields and Childhood Leukaemia", Br J Cancer, vol. 103, pp. 1128-1135, 2010.

[5] World Health Organization, Extremely Low Frequency Fields, Environmental Health Criteria No. 238, Ed. Geneva, Switzerland: WHO Press, 2007.

[6] Scientific Committee on Emerging and Newly Identified Health Risks (SCENIHR), Preliminary Opinion on Potential Health Effects of Exposure to Electromagnetic Fields (EMF), Luxembourg: European Commission, 2013.

[7] J. Schüz, "Exposure to Extremely Low-Frequency Magnetic Fields and the Risk of Childhood Cancer: Update of the Epidemiological Evidence", *Prog. Biophys. Mol. Biol*., vol. 107, pp. 339-342, Dec. 2011.

[8] L. Kheifets, S. Oksuzyan, "Exposure Assessment and Other Challenges in Non-Ionizing Radiation Studies of Childhood Leukemia". *Radiat. Prot. Dosimetry*, vol. 132, pp. 139-147, 2008.

[9] *TransExpo: International Study of Childhood Leukemia and Residences Near Electrical Transformer Rooms. Palo Alto, CA (USA): EPRI 3002001085, 2013.*

[10] S. Lagorio, A. Polichetti, L. Bisanti. TransExpo feasibility in Italy. In: II Convegno nazionale ICEmB. Interazioni fra campi elettromagnetici e biosistemi. Atti; 27-29 giugno 2012; Bologna. 2012.

[11] K. Ilonen et al., "Indoor transformer stations as predictors of residential ELF magnetic field exposure". *Bioelectromagnetics*, vol. 29, pp. 213-218, 2008.

[12] G. Thuroczy et al., "Exposure to 50 Hz magnetic field in apartment buildings with built-in transformer stations in Hungary", *Radiat. Prot. Dosimetry*, vol. 131, pp. 469-473, 2008.

[13] R. Hareuveny et al., "Exposure to 50 Hz magnetic fields in apartment buildings with indoor transformer stations in Israel". *J. Expo. Sci. Environ. Epidemiol*., vol. 21, pp. 365-371, 2011.

[14] M. Röösli et al., "Extremely low frequency magnetic field measurements in buildings with transformer stations in Switzerland". Sci. Total Environ.vol. 409, pp. 3364-3369, 2011:

[15] A. Huss et al., "Does apartment's distance to an in-built transformer room predict magnetic field exposure levels?". *J. Expo. Sci. Environ. Epidemiol*., vol. 23, pp. 554-558, 2013.

General public co-exposure to electromagnetic fields and radon in urban environment

R. Massa[1,2,3] , M. Pugliese[1,2], M. Quarto[2], V. Roca[1,2], S. Romeo[3], O. Zeni[3]
[1]*National Institute of Nuclear Physics (INFN)-Sez.Naples*
[2] *Dept. of Physics, University of Naples Federico II, via Cinthia, 80126, Naples, Italy*
[3]*CNR – Institute for Electromagnetic Sensing of the Environment (IREA), via Diocleziano 328, 80124, Naples, Italy*

***Abstract*— Results of a measurement campaign in urban environment near Naples for monitoring the co-exposures of the population to electric, magnetic and electromagnetic fields and radon will be presented. Measurements were carried out in towns rich in rocks of tuffs and pyroclastics that are major source of radon and in particular in sites where prolonged presence of children and teenagers is foreseen.**

I. INTRODUCTION

Electromagnetic fields (EMF) including both radiofrequency radiation (RF) used by mobile phones and new wireless technologies, and extremely low frequency (ELF) due to the generation, transmission, and use of electricity represent ubiquitous sources of daily exposure of the general public. As a consequence, population exposure to EMF is a great scientific interest issue, for which a proper assessment is decisive for a correct awareness and risk perception. Being an ubiquitous source of exposure, it is interesting to consider combined exposure to EMF and other environmental pollutants. In this framework, combined exposures to EMF and radon and its progeny, which contribute more than half to human exposure to ionizing radiation from natural sources, are considered. As a matter of fact, Radon (^{222}Rn) is a natural radioactive noble gas produced from the decay series of ^{238}U, and for this reason its distribution is very variable in the earth's crust. ^{222}Rn and its progenies in air constitute the major natural exposure source to ionizing radiation for humans [1] because it can accumulate in enclosed space. International Agency for Research on Cancer (IARC) [2] has defined radon as a human carcinogen since 1988 and EPA 2003 [3] has reported that the radon is the second risk factor for lung cancer after smoking. The International Commission on Radiological Protection (ICRP) [4] has established an action levels between of 400 Bq/m^3 and 600 Bq/m^3. In Italy, the authorities, had adopted as action level of 400 Bq/m^3 for existing houses and 200 Bq/m^3 for future buildings in accordance with international recommendation [4].

In this work, the results of a measurement campaign carried out in several small towns of the Penisola Sorrentina, an area rich of rich in rocks of tuffs and pyroclastics, will be reported, in order to characterize combined exposure of the general public to both eletromagnetic fields and radon.

II. MATERIALS AND METHODS

A. Electromagnetic fields measurements

Electromagnetic fields (EMF) measurements at extremely low frequencies (ELF) were carried out by means of a broad band instrumentation which included the Narda EFA 300 radiation meter, a magnetic and an electric field probe (5 Hz – 32 kHz), a tripod made by dielectric material. Both instantaneous magnetic induction values at 50 Hz and frequency spectra were acquired at each measurement point (6% extended uncertainty, k = 2).

EMF measurements at radiofrequencies (RF) were performed by means of both broadband and narrow band instrumentations. The PMM 8053 radiation meter (Narda), equipped with a EP-330 electric field probe were used for broadband measurements in the range from 100 kHz to 3 GHz (27% extended uncertainty, k = 2)

Narrow band measurements were carried out by means of the test system shown in Figure 1, which included: 1) an isotropic TS-EMF B1 probe (30 MHz – 3 GHz, Rohde & Schwarz); 2) a FSH-8 spectrum analyzer (100 kHz – 8 GHz, Rohde & Schwarz); 3) a computer installed with the RFEX v.1.6.34 (R&S) software for the remote control of measurement instrument and the antenna switching, for the integration and correction of the measurement data, for data saving and report generation. The software is provided with several measurement packets which define the operating conditions of the spectrum analyzer to detect emissions from different radiation sources (e.g., TV and radio broadcasting, mobile phone base stations…) in a certain frequency range. In the present work, measurement configurations associated to GSM, UMTS, WiFi packets were adopted (extended uncertainty 30-40%, k = 2, depending on the measurement packet).

Fig. 1 Test system for RF, narrow-band electromagnetic fields measurements.

B. Indoor radon concentration measurements

The technique used in this study is based on long-term measurement with passive alpha detectors (SSNTDs) LR-115. In each dwelling, two detectors were exposed in the rooms were the inhabitants spent the most of their time, generally the living room and bedroom, for two consecutive semesters in order to obtain a whole year of exposure. After exposure all detectors were chemically etched using a solution of 2.5 N NaOH at 60 °C for 110 min and scanned. The recorded track density was then converted in radon concentration using a suitable calibration factor.

TABLE I

RESULTS OF 50 HZ MAGNETIC FIELD (BROADBAND), RADIOFREQUENCY (NARROW BAND, GSM, UMTS AND WLAN PACKETS) AND RADON INDOOR MEASUREMENTS IN TWO TOWNS OF THE PENISOLA SORRENTINA ([A] WLAN SOURCE IN THE MEASUREMENT ROOM; [B] WLAN SOURCE IN A ROOM ADJACENT TO THE MEASUREMENT ONE)

Sant'Agnello					
n.	**B @ 50 Hz [nT]**	**GSM900 [V/m]**	**UMTS [V/m]**	**WLAN [V/m]**	**Radon [Bq/m^3]**
1	30	0.066	0.076	0.045 [B]	455 ± 10
2	100	0	0	0.029 [B]	113 ± 1
3	40	0.016	0	0 [B]	109 ± 3
4	80	0.021	0.023	1.210 [A]	168 ± 6
5	227	0	0	0 [B]	82 ± 1
6	20	0	0.006	0.064 [B]	101 ± 10
7	70	0	0.017	0.368 [A]	71 ± 4
Piano di Sorrento					
8	80	0	0.020	0.049 [B]	165 ± 28
9	40	0	0.116	0.778 [A]	94 ± 1
10	10	0	0.006	0.045 [A]	84 ± 5

III. RESULTS AND DISCUSSION

The indoor radon concentrations measured in the dwellings of *Penisola Sorrentina* are reported in Table I. The results show that in 90% of houses, the radon concentrations are below 200 Bq/m^3, that is the recommended level of Italian legislation for new buildings and only 10% are higher than 400 Bq/m^3 which is the recommended level of Italian legislation for old building.

As far as the results of electromagnetic field measurements are concerned, magnetic induction levels at 50 Hz were always below the exposure limits (100 μT), the attention level (10 μT) and threshold value (3 μT) defined by the Italian law (Table I). The same holds true for both broadband and narrow band measured radiofrequency electric field levels. Interestingly, from the narrow band radiofrequency measurements, it turned out that the major contribution came from Wi-Fi signals (Table I). Moreover, measured results were in agreement with those of similar measurement campaigns carried out in other European countries [5].

ACKNOWLEDGEMENTS

The authors thank Prof. R. Ortenzia and the residents of the study area for their collaboration to the project, and Dr Giuseppe Scognamiglio for performing part of the measurements. In addition, the authors thank the Rhode & Schwartz for the technical assistance.

REFERENCES

[1] United Nations, "United Nations Scientific Committee on the Effects of Atomic Radiation (UNSCEAR). Sources, Effects and risks of ionizing radiation," 2000.

[2] International Agency for Research on Cancer (IARC), "Monographies on the Evaluation of Carcinogenic Risks to Humans," vol. 43, pp. 173-259, 1988.

[3] United States Environmental Protection Agency (US EPA), "Assessment of risk from radon in homes," EPA 402-R- 03- 003, 2003.

[4] International Commission on Radiological Protection, *Protection against radon at home and work*, ICRP Publication 65. Ann. ICRP vol. 23(2), Pergamon Pres, 1993.

[5] L. Kheifets, M. Repacholi, R. Saunders, E. van Deventers, "The Sensitivity of Children to Electromagnetic Fields," *Pediatrics*, vol. 116: e303-e313, 2005

Dielectric and Thermal Properties of Tissues Undergoing Microwave Thermal Ablation Procedures

Laura Farina[*], Vanni Lopresto[+], Rosanna Pinto[+], Marta Cavagnaro[*]

[*]*Department of Information Engineering, Electronics and Telecommunications, Sapienza University of Rome, Via Eudossiana 18, 00184 Rome, Italy, farina@diet.uniroma1.it*

[+]*Technical Unit of Radiation Biology and Human Health, Casaccia Research Centre, ENEA, Rome, Italy*

***Abstract* – In this paper a review of the studies devoted to the characterization of the dielectric and thermal properties of tissues treated with a microwave thermal ablation procedure is conducted. The state of the art, measurement set-ups and techniques, experimental results, and developed computational/numerical models will be presented, and future research needs identified.**

I. Introduction

Thermal ablation therapies exploit the interaction between a physical energy and a biological tissue to heat the target cells up to irreversible injury; microwave (MW) thermal ablation uses the electromagnetic (EM) field radiated by a minimally invasive antenna in the MW frequency range (typically 915 MHz or 2.45 GHz) as heat source [1].

Raising the biological tissue temperature to values higher than 42 °C, increases susceptibility to damage by other mechanisms (e.g. radiation or chemotherapy). Permanent cellular damage occurs after 60 minutes at 46 °C, and after only 4 - 6 minutes at 50 - 52 °C. Increasing the temperature over about 60°C leads almost instantaneous cellular death due to protein denaturation, which irreversibly alters the tissue's structure and properties (both dielectric and thermal) [2, 3]. Over 100 °C, the tissue boils, vaporizes and carbonizes [4].

Information on the temperature distribution and on temperature-dependent thermal and dielectric properties of the target tissue are fundamental to evaluate the EM power deposition and the heat conduction within the tissue, and, consequently, to determine the achievable size of the thermal lesion. The EM power deposition and the corresponding temperature increase can be modelled by the Maxwell's equations (1) and by the bio-heat transfer equation (2), reported below.

$$(1)\quad \begin{cases} \nabla\times\boldsymbol{E}(\boldsymbol{r},\omega) = -j\omega\mu(\boldsymbol{r},\omega)\boldsymbol{H}(\boldsymbol{r},\omega) \\ \nabla\times\boldsymbol{H}(\boldsymbol{r},\omega) = \sigma\boldsymbol{E}(\boldsymbol{r},\omega) + j\omega\varepsilon(\boldsymbol{r},\omega)\boldsymbol{E}(\boldsymbol{r},\omega) + \boldsymbol{J}_i(\boldsymbol{r},\omega) \end{cases}$$

$$(2)\quad C(\boldsymbol{r})\rho(\boldsymbol{r})\frac{\partial T}{\partial t} = \\ = \nabla\cdot(k(\boldsymbol{r})\nabla T) + A_0(\boldsymbol{r}) + Q_v(\boldsymbol{r}) - B_0(\boldsymbol{r})(T - T_b)$$

Their solution is strongly dependent on the values of the tissue dielectric (permittivity ε, and conductivity σ) and thermal (specific heat capacity C, and thermal conductivity k) properties, as well as on the EM field (vector electric $\boldsymbol{E}$ and magnetic $\boldsymbol{H}$ fields, and incident current density $\boldsymbol{J}_i$, all dependent on the spatial position $\boldsymbol{r}$ and on the frequency f, with $\omega=2\pi f$) and on the tissue density ρ and temperature T. In equation (2) there is also the contribution of the external heat source (Q_v), the metabolic heat generation (A_0) and the blood perfusion (B_0, with T_b the blood temperature).

While the dielectric and thermal properties in (1) and (2) at temperatures close to those of the human body have been widely studied, less researches have been conducted considering the high temperature values typical of MW thermal ablation. Moreover, the higher the tissue temperature, the more difficult the comprehension of the changes in the tissue properties is.

In the following, the literature works investigating the dielectric and thermal properties of biological tissues will be reviewed, with particular attention to their changes in correlation with the temperature.

II. Dielectric Properties of Biological Tissue

Several authors investigated the changes in the relative permittivity and conductivity of *ex vivo* tissue with the temperature [2, 4 - 11]. However, only two groups focused on microwave thermal ablation procedures [12 - 14].

In these studies, the tissue dielectric properties were measured in *ex vivo* tissues undergoing MW thermal ablation, by the open-ended coaxial probe technique. Tissue's temperature was also monitored, using either thermocouple or fibre-optic probes, in order to infer a correlation between the changes in the dielectric properties and the temperature increase. In [12], the temperature and the dielectric properties were measured at the same location, bundling the temperature sensor with the dielectric probe, and positioning them parallel to the MW antenna. In [13, 14], the tissue's temperature and the dielectric properties were measured in different locations, positioning the probes perpendicularly to the antenna's axis at the same radial distances, exploiting the cylindrical symmetry of the antenna, and supposing the tissue to be homogeneous.

Both in [12] and in [14], sigmoid correlations between the temperature gradient and the changes in the dielectric properties of the tissue have been established. Accordingly, as the temperature reaches values close to 60 °C, the tissue's dielectric properties drop very rapidly. However, the models proposed by the two research groups show significant differences in the dielectric properties values over the range 80 °C – 100 °C, with differences as high as 100%. In [14], it has been pointed out that the changes in the tissue's dielectric properties strictly depend on the local temperature reached and, thus, on the amount of MW energy delivered punctually to the tissue. Consequently, tissue's dielectric properties vary spatially as a function of the temperature gradient in the thermal lesion.

III. Thermal Properties of Biological Tissue

Researches investigating the thermal properties of biological materials are less prevalent in literature. The changes in the thermal parameters of the tissue were investigated mostly near normal body temperature [15, 16].

In [17, 18], the temperature changes in *ex vivo* tissue undergoing MW ablation were measured, and the direct link between the temperature increment and the changes in the

tissue's water content was investigated. The experimental results were used to develop an improved numerical model, defining a modified bio-heat equation; an effective specific heat, that considers the water content and thereby is function of the temperature, was implemented.

Other studies were conducted on *ex vivo* tissue sample exploiting the transient line heat source technique, deploying *ad hoc* probes [19] or commercial devices [20]. The line heat source technique consists in obtaining the thermal conductivity of the medium from the time-rate evolution of the temperature of a very thin metallic wire placed into the medium. The wire is heated applying a step voltage, thus obtaining an essentially uniform line source of heat flux per unit length [21]. The rise in temperature of the wire is dependent on the thermal conductivity of the surrounding medium [22].

In [19], the thermal conductivity of different tissues (*in vitro* sheep collagen and *in vitro* cow liver) were measured as a function of the temperature with subsequent experiments in the range of 25- 90 °C, by heating the samples in a water bath. In both tissues, irreversible changes in the thermal conductivity were observed beyond a threshold temperature (55 °C for the collagen and 90 °C for the liver). Moreover, the thermal conductivity was measured *in vivo* in pig forelimb (across and along strands), neck (fat) and liver, pointing out the major role played in heat dissipation by the blood perfusion.

In [20], the specific heat capacity, the thermal conductivity, and the heat diffusivity of *ex vivo* tissue samples were evaluated as function of the temperature, between 20 °C and 90 °C, investigating both the heating and the cooling phenomena within a water bath. The thermal properties changed as function of the temperature with a decreasing trend between 20 °C and 35 - 40 °C, where a minimum was reached (3.567 mJ/(m^3·K) at 35 °C, for the thermal conductivity), and then with an increasing trend up to 90 °C following a quasi-parabolic behaviour (4.296 mJ/(m^3·K) at 90 °C). Moreover, the irreversible structural changes of the biologic tissue after reaching necrotic temperatures was highlighted, since the observed properties could not recover on cooling.

CONCLUSIONS

The changes of the dielectric properties of biological tissues with the temperature have been deeply investigated in the literature. These studies highlighted that the dielectric changes are linked to the temperature only, not to the heating modality or duration, and vary spatially, due to the temperature gradient induced into the tissue by the heating process. Nevertheless, further researches are required to better characterize the tissue behaviour at the highest temperatures (> 100 °C), where complex phenomena related to both physical (e.g. water vaporisation) and morphologic modifications (e.g. tissue contraction) occur.

Regarding the thermal properties of the biological tissues, their dependence from the temperature is settled. Yet the knowledge of the underlying mechanisms and related phenomena is limited: therefore more researches are essential to gain further insight.

Additionally, the changes in the tissue's density should also be considered, since they are strictly involved in the shrinkage phenomenon observed during the MTA.

BIBLIOGRAFIA

[1] M. Ahmed, C.L. Brace, F.T. Lee FT, S.N. Goldberg. "Principles of and advances in percutaneous ablation", *Radiology*, vol. 258, pp.351-69, 2011.

[2] L. Chin and M. Sherar, "Changes in dielectric properties of ex vivo bovine liver at 915 MHz during heating," *Phys Med Biol*, vol. 46, pp. 197-211, 2001.

[3] C. Bircan and S.A. Barringer, "Determination of protein denaturation of muscle foods using the dielectric properties," *J Food Sci.*, vol. 67, pp. 202-205, 2002.

[4] C.L. Brace, "Temperature-dependent dielectric properties of liver tissue measured during thermal ablation: toward an improved numerical model," in *Conf. Proc. IEEE Eng. Med. Biol. Soc*., 2008, pp 230–233.

[5] C.C. Johnson and A.W. Guy, "Non-ionising electromagnetic wave effects in biological materials and systems," *Proc. IEEE*, vol.66, pp. 692–718, 1972.

[6] K.R. Foster, J.L. Schepps, R.D. Stoy and H.P. Schwan, "Dielectric properties of brain tissue between 0.01 and 10 GHz," *Phys. Med. Biol.*, vol. 24, pp. 1177-1187, 1979.

[7] K.R. Foster and H.P. Schwann, "Dielectric properties of tissues and biological materials: a critical review," *Crit. Rev. Biomed. Eng.*, vol. 17, pp. 25-104, 1989.

[8] S. Ryynanen, "The electromagnetic properties of food materials: a review of basic properties," *J. Food Eng.*, vol. 26, pp. 409-429, 1995.

[9] L. Chin and M. Sherar, "Changes in the dielectric properties of rat prostate *ex vivo* at 915 MHz during heating," *Int. J. Hyperth.*, vol. 20, pp. 517-527, 2004.

[10] P.R. Stauffer, F. Rossetto, M. Prakash, D.G. Neuman and T. Lee, "Phantom and animal tissues for modeling the dielectric properties of human liver," *Int. J. Hyperth.*, vol. 19, pp. 89-101, 2003.

[11] M. Lazebnik, M.C. Converse, J.H. Booske and S.C. Hagness, "Ultrawideband temperature-dependent dielectric properties of aninal liver tissue in the microwave frequency range," *Phys. Med. Biol.*, vol. 51, pp. 1941-1955, 2006.

[12] Z. Ji and C.L. Brace, "Expanded modeling of temperature-dependent dielectric properties for microwave thermal ablation," *Phys Med Biol*, vol. 56, pp. 5249-5264, 2011.

[13] V. Lopresto, R. Pinto, G.A. Lovisolo, and M. Cavagnaro, "Changes in the dielectric properties of ex vivo bovine liver during microwave thermal ablation at 2.45 GHz," *Phys Med Biol*, vol. 57, pp. 2309-2327, 2012.

[14] V. Lopresto, R. Pinto, and M. Cavagnaro, "Experimental characterization of the thermal lesion induced by microwave ablation," *Int J Hypertermia*, vol. 30, pp. 110-118, 2014.

[15] J.W. Valvano, J.R. Cochran, K.R. Diller, "Thermal conductivity and diffusivity of biomaterials measured with self-heating thermistors," *Int J Thermophys*., vol.6, pp. 301-311, 1985.

[16] D. Haemmerich, I. Santos, D.J. Schutt, J.G. Webster, D.M. Mahvi, "In vitro measurements of temperature-dependent specific heat of liver tissue," *Med Eng Phys*., vol. 28, pp. 194-197, 2006.

[17] D. Yang, M.C. Converse, D.M. Mahvi, and J.G Webster, "Measurement and analysis of tissue temperature during microwave liver ablation," *IEEE Trans Biomed Eng*, vol. 54, pp. 150-155, 2007.

[18] D. Yang, M.C. Converse, D.M. Mahvi, and J.G Webster, "Expanding the bioheat equation to include tissue internal water evaporation during heating," *IEEE Trans Biomed Eng*, vol. 54, pp. 1382-1388, 2007.

[19] A. Bahattacharya and R.L. Mahajan, "Temperature dependence of thermal conductivity of biological tissues," *Physiol Meas*, vol. 24, pp. 769-783, 2003.

[20] S.R. Guntur, K.I. Lee, D-G. Paeng, A.J. Coleman, and M.J. Choi, "Temperature-dependent thermal properties of *ex vivo* liver undergoing thermal ablation," *Ultrasound in Med & Biol*, vol. 39, pp.1771-1784, 2013.

[21] M.J. Assael, K.D. Antoniadis and W.A. Wakeham, "Historical evolution of the transient hot-wire technique," *Int J Thermophys.*, vol. 31, pp. 1051-1072, 2010.

[22] S. Alvarado, E. Marin, A.G. Juarez, A. Calderon and R. Ivanov, "A hot-wire method based thermal conductivity measurement apparatus for teaching purposes," *Eur J Phys.*, vol. 33, pp. 897-906, 2012.

Modelling of Deep Trascranial Magnetic Stimulation: Electric Field Distributions Induced in a Realistic Human Model by Different Coil Designs

V. Guadagnin[1], M. Parazzini[1], S. Fiocchi[1], I. Liorni[1,2] and P. Ravazzani[1]

[1]*Istituto di Elettronica e di Ingegneria dell'Informazione e delle Telecomunicazioni, IEIIT-CNR, Piazza Leonardo da Vinci, 32, 20133 Milano, Italy*

[2]*DEIB, Politecnico di Milano, Piazza Leonardo da Vinci, 32, 20133 Milano, Italy*

***Abstract*—This paper investigates the induced electric field distributions in a realistic human head model due to 16 coil configurations. We used the scalar potential finite element method differentiating the brain structures. We found that, despite the presence of a depth-focality tradeoff, some coils are able to reach subcortical white matter tracts at effective electric field level.**

I. Introduction

Transcranial magnetic stimulation (TMS) is a non-invasive technique of neurostimulation based on the principle of electromagnetic induction of an electric field in the brain [1]. This field is able to modulate the transmembrane potentials of neuronal cells and, as a result, their activity. Recently, there has been an increasing interest in extending the TMS to deep brain region [2], with the consequences that new coils design have been developed [3]. In the meantime, several clinical studies showed that deep transcranial magnetic stimulation (DTMS) could be more effective than TMS in treating a very wide range of neurological, psychiatric and medical conditions, e.g. major depressive disorder, schizophrenia, bipolar depression, post-traumatic stress disorder, obsessive-compulsive disorder and substance addictions [4]. The region that is activated in the brain corresponding, approximately, with the areas in which the induced electric field (**E**) is maximum [3]. The location of these regions depends on the coil geometry and on its position on the scalp. Thus, the knowledge of the induced **E** distributions and the comparison between the different configurations of coils are indispensable in order to evaluate the experimental results and to optimize the therapeutic treatments. Despite the increasingly interest in this technique and the rising number of clinical applications [4], little has been done so far to quantify the induced **E** distributions in the brain due to different configuration of coil used for DTMS. Indeed, until now, these distributions have been estimated or using simplified head geometric models, such as sphere [3], or considering each coil separately and without a comparison among different coil configurations [5]. The aim of this study, therefore, consists in characterizing and comparing the induced **E** distributions in the brain of a realistic human head model by different configurations of coils for TMS and DTMS by mean of quantitative and comparative parameters.

II. Materials and Methods

A. Coil designs

Fig. 1 shows the 16 different coil configurations modelled in this study: two designs represent the references and are constituted by the circular coil and the figure-8 coil, the other 14 are chosen because identified by the clinical literature as the most effective for DTMS [3].

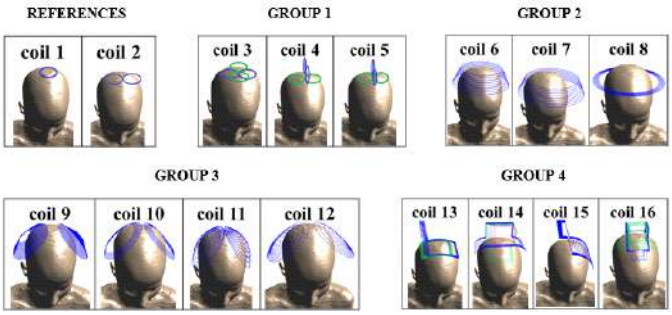

Figure 1. 16 different coil configurations modelled divided into groups based on common geometric characteristics and placed on the head of the anatomical model "Ella".

They are composed of a group of coils characterized by two pairs of figure-8 coil arranged according to different orientations on the scalp (group 1), of the category of large diameter circular coils (group 2), of the family of double cone coils (group 3), formed by two large adjacent circular windings fixed at different angles on the scalp, and of the group of H coils (group 4), consisting of complex three-dimensional pattern of windings [5], [6].

B. Simulations

The simulations were performed on the head of the realistic anatomical model "Ella" (a 26-years old female), of the Virtual Family [7]. The dielectric properties of each tissue were assigned based on the literature data at low frequency [8], [9]. Simulations were conducted using the magneto quasi-static low-frequency solver of the simulation platform SEMCAD X (by SPEAG, www.speag.com) [10]. With the purpose to compare the different coils configurations, in all the simulations a pulse current with amplitude of 1 A and a frequency of 5 kHz were used.

C. Coil performance metrics

For each coil, the **E** distributions were computed and analyzed in different brain structures. In each brain tissue, we estimated the percentage of volume that had **E** values equal to or greater than 10%-90% of the 99th percentile of the **E** distribution in the cortex. We also evaluated the **E** penetration depth by comparing the field values, normalized to the 99th percentile of the cortical **E**, at the distances of 1 cm, 2 cm, 3 cm and 4 cm from the cortical surface both on frontal slices common to all the coils and on the frontal slices in which each coil reaches its maximum penetration depth. Moreover, we estimated the average distance from the cortical surface of the

50% of the 99th percentile of the **E** in the cortex of each coil on the frontal and on the sagittal planes.

III. Results

Fig. 2 shows some examples of the **E** distributions in the brain due to some coils (i.e. the two reference coils and one for each group of DTMS coil configurations).

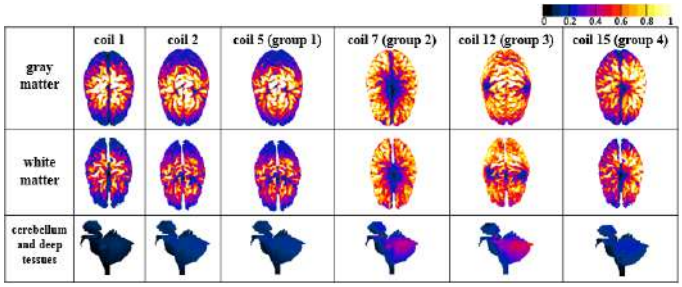

Figure 2. Surface distributions of the induced **E** in the cortex (1st row), white matter (2nd row) and cerebellum with deep brain tissues (3rd row) for the reference coils and for one coil of each group. The field amplitudes are normalized respect to the 99th percentile of the **E** distribution in the cortex.

In each panel the values are normalized with respect to the 99th percentile of the **E** distribution estimated on the cortex. These panels clearly show that varying the coil configurations induces variations in the **E** distributions in all the brain structures. More interestingly, it shows that only few coils (belonging to group 2 and 3) are able to reach deep brain structures (hippocampus, pons, midbrain, thalamus and hypothalamus), with **E** values ranging between the 20-30% of the maximum in the cortex.

As to the **E** penetration depth, Fig. 3 shows the trend of **E** as a function of distance from the cortical surface for each coil configuration.

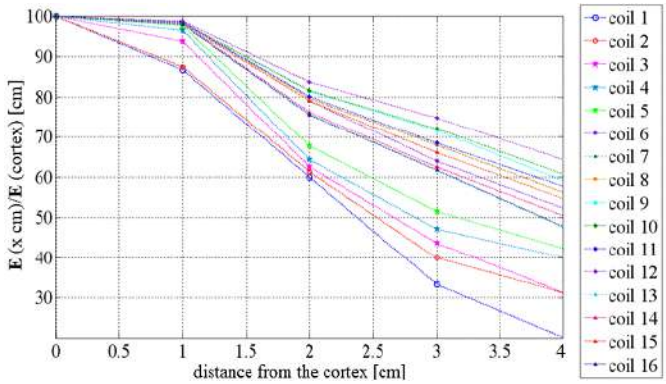

Figure 3. **E** values, normalized respect to the 99th percentile of the **E** distribution in the cortex, at increasing distance from the cortical surface, for the 16 coil configurations on the frontal slices in which each coil reaches its maximum penetration depth.

The **E** values are normalized respect to the 99th percentile of the **E** distribution in the cortex, evaluated for each coil configuration. It can be seen that the rate of decay of **E** with distance is significantly quicker for the reference coils, especially for the circular coil, and for the coils of the first group compared to the other configurations. In fact, the **E** values of these first coils at a depth of 4 cm are equal to 30-40% of the maximum and to 20% of the maximum for the circular coil. The coils belonging to the second and to the third group attenuate the degree of reduction of the induced **E** with the increase of distance: the **E** values at a depth of 4 cm are respectively equal on average to 55% and to 60% of the maximum. At last, the **E** decay profile as a function of distance from the cortical surface of the H coils (group 4) is more slower than the references and than the first group, but faster than the second and than the third group of coils. Indeed, the **E** values at a depth of 4 cm ranging between 47% and 55% of the maximum. In the case of the single circular coil, the average distance from the cortical surface of the 50% of the 99th percentile of the **E** evaluated in the cortex on different frontal and sagittal planes is approximately equal to 2 cm. For the figure-8 coil and for the coils belonging to the first group it is below 3 cm. The coils of the second group, on the other hand, increase the average depth of the 50% of the 99th percentile of the **E** in the cortex, up to 3.5 cm. The coils belonging to the third group are characterized by the highest depth values, ranging between 3.5 cm and 4.5 cm, on both planes. Finally, for the coils of the fourth group the average depth on both the planes ranges between 3 cm and 3.5 cm.

IV. Conclusion

This study shows that some configurations (particularly the H coils of group 4) result to be able to reach effective stimulation of subcortical white matter tracts. On the contrary, few coils are able to reach deeper brain structures with **E** values greater than 20% of the maximum. In conclusion, this study shows how the characterization of the **E** distributions could play an important role in the optimization of the geometry and of the position on the scalp of the coils and can help clinicians in the choice of the coil more suitable to fulfil the needs of a specific treatment.

References

[1] A. T. Barker, R. Jalinous and I. L. Freeston, "Non-invasive magnetic stimulation of human motor cortex", Lancet, vol. 1, pp. 1106-1107, 1985.

[2] Y. Roth, F. Padberg, A. Zangen, "Transcranial magnetic stimulation of deep brain region: principles and methods", Adv. Biol. Psychiatry, vol. 23, pp. 204-224, 2007.

[3] Z. D. Deng, S. H. Lisanby, A. V. Peterchev, "Electric field depth-focality tradeoff in transcranial magnetic stimulation: simulation comparison of 50 coil design", Brain Stimul., vol. 6, pp. 1-13, 2013.

[4] F. S. Bersani, A. Minichino, P. G. Enticott, L. Mazzarini, N. Khan et al., "Deep transcranial magnetic stimulation as a treatment for psychiatric disorders: a comprehensive review", Eur. Psychiatry, vol. 28(1), pp. 30-39, 2013.

[5] Y. Roth, A. Amir, Y. Levkovitz, A. Zangen, "Three-dimensional distribution of the electric field induced in the brain by transcranial magnetic stimulation using figure 8 and deep H-coils", J. Clin. Neurophysiol., vol. 24, pp. 31-38, 2007.

[6] A. Zangen, Y. Roth, B. Voller, M. Hallet, "Transcranial magnetic stimulation of deep brain regions: evidence for efficacy of the H-coil", Clin. Neurophysiol., vol. 116, pp. 775-779, 2005.

[7] A. Christ, W. Kainz, E. G. Hahn, K. Honegger, M. Zefferer et al., "The virtual family- development of surface-based anatomical models of two adults and two children for dosimetric simulations", Phys Med. Biol., vol. 55, pp. N23-N38, 2010.

[8] S. Gabriel, R. W. Lau, C. Gabriel, "The dielectric properties of biological tissues: II. Measurements in the frequency range of 10 Hz to 20 GHz", Phys Med. Biol., vol. 41, pp. 2251-2269, 1996b.

[9] C. Gabriel, A. Peyman, E. H. Grant, "Electrical conductivity of tissue at frequencies below 1 MHz", Phys Med. Biol., vol. 54, pp. 4863-4878, 2009.

[10] SEMCAD X v14.8 by SPEAG, Available at www.speag.com.

Computational Modeling of Transcranial Direct Current Stimulation: Effect of Human Anatomical Variability

Marta Parazzini[1], Serena Fiocchi[1], Ilaria Liorni[1,2], Vanessa Guadagnin[1], Alberto Priori[3,4], Paolo Ravazzani[1]

[1]*CNR Consiglio Nazionale delle Ricerche, Istituto di Elettronica e di Ingegneria dell'Informazione e delle Telecomunicazioni IEIIT, 20133 Milano, Italy; marta.parazzini@ieiit.cnr.it*

[2]*Dipartimento di Elettronica, Informazione e Bioingegneria, Politecnico di Milano, 20133 Milano, Italy;*

[3]*Dipartimento di Fisiopatologia Medico-Chirurgica e dei Trapianti, Università degli Studi di Milano, 20122 Milano, Italy;*

[4]*Centro Clinico per la Neurostimolazione, le Neurotecnologie ed i Disordini del Movimento, Fondazione IRCCS Ca' Granda Ospedale Maggiore Policlinico, 20122, Milano, Italy*

Summary - **This paper investigates how normal variations in anatomy may affect the current flow through the brain due to transcranial direct current stimulation. This was done by comparing the electric field and current density distributions within the tissues obtained in human models of different age and sex.**

I Introduction

Transcranial direct current stimulation (tDCS) is a non-invasive brain stimulation technique that utilizes low intensity direct current to modulate brain excitability [1]. The increasingly widespread use of this technique and the rising number of clinical applications have boosted the interest in the estimation of the levels of the electric quantities in the brain tissues due to tDCS. As a consequences, there has been an increase of publications aiming to quantify the spatial distribution of the electric field (**E)** and of the current density (**J)** within the human brain tissues during tDCS, [for a review, see, 2-3]. Since the most of these studies are based on one single head model, it is still unknown how and if the human variability may affect the current flow through the tissues and particularly in the brain.

Aim of this paper is to contribute in filling this gap in knowledge, assessing the effect of the anthropometric variables of the subject, of his/her morphological and anatomical characteristics on the spatial distribution of **E** and **J** within cortical and subcortical brain structures, considering different electrode montages.

II Materials and Methods

Simulations were conducted using the simulation platform SEMCAD X (by SPEAG, www.speag.com), solving the Laplace equation to determine the electric potential distribution inside all the human tissues.

Three realistic human models of the Virtual Family [4] ("Ella": a 26-years-old female; "Duke": a 34 years-old male; "Billie": an 11 years old female) were used in the study. The dielectric properties of the tissues were assigned on the basis of the literature data at low frequency [5-6].

Four electrode montages were modeled: 1) *Montage A*: one electrode was placed on F3 and one on F4, as in [7]; 2) *Montage B*: one electrode was placed on T3 and the reference on the right arm, as in [8]; 3) *Montage C*: two electrodes were placed on C3 and C4, whereas the reference was on the right arm, as in [9]; 4) *Montage D*: one electrode was placed on Fz and the reference on the right tibia, as in [10]. In all the electrode montages described above, F3, F4, T3, C3, C4 and Fz were referred to the 10-20 EEG system. The potential difference between the electrodes was adjusted to inject a total current of 1 mA in all the four electrode montages. For all the montages and the human models, the spatial amplitude distributions of **E** and **J** were analyzed in cortical and subcortical brain regions. For the gray and white matter, we also calculated the percentage of volume where the amplitude of **E** (or **J**) was greater than 70% or 50% of its peak. These percentages of volume will be named in the following sections as V70 or V50, respectively. To assess if there were any significant changes in the percentage of volume V70 or V50 due to the human anatomical variability, the Kruskal–Wallis one-way analysis of variance by ranks was performed. The human model was the only factor with three levels ("Ella", "Duke" and "Billie"). If *human model* factor was significant, a Mann-Whitney non-parametric post-hoc multiple comparison test, with a Bonferroni adjustment to the criterion of significance, was also performed to assess which pairs of groups differ significantly from one another.

The influence of the human variability on the field values was assessed evaluating the coefficient of variability (i.e., the ratio between the standard deviation and the mean, expressed in dB) among the models of both the peak and of the median of **E** ($\mathbf{E}_{peak}$ and $\mathbf{E}_{median}$) in the cortical and subcortical brain regions, for all the electrode montages.

III. Results

Figure 1 shows the normalized amplitude distribution of **E** (or **J**) on different sections across the gray matter for the four electrode montages using "Billie" as an example. A qualitative comparison of these panels immediately indicates that varying the electrodes montage induces different spatial distribution of the amplitude of **E** (or **J)** in the gray matter. Interestingly for all the models, the symmetric electrode montages (Montage A and C) tend to have comparable amplitude of **E/J** in both hemispheres, while the lateralized electrode configuration (Montage B) generates higher amplitude of **E/J** asymmetrically in one hemisphere only. Similarly, configurations with anterior electrodes (Montage A and D) induce higher amplitude of both **E** (and **J**) in the anterior portion of the brain. The spread of the amplitude distribution over the gray and white matter, quantified as V70 or V50 resulted very similar across the human models. Indeed, statistical analysis on both V70 and V50 shows that the *human model* factor was not statistically significant (p-value>0.05) for all the electrode montages. The combination of human

model and electrode montage that shows the more focalized spatial distribution of both **E** (and **J**) is always the Montage A

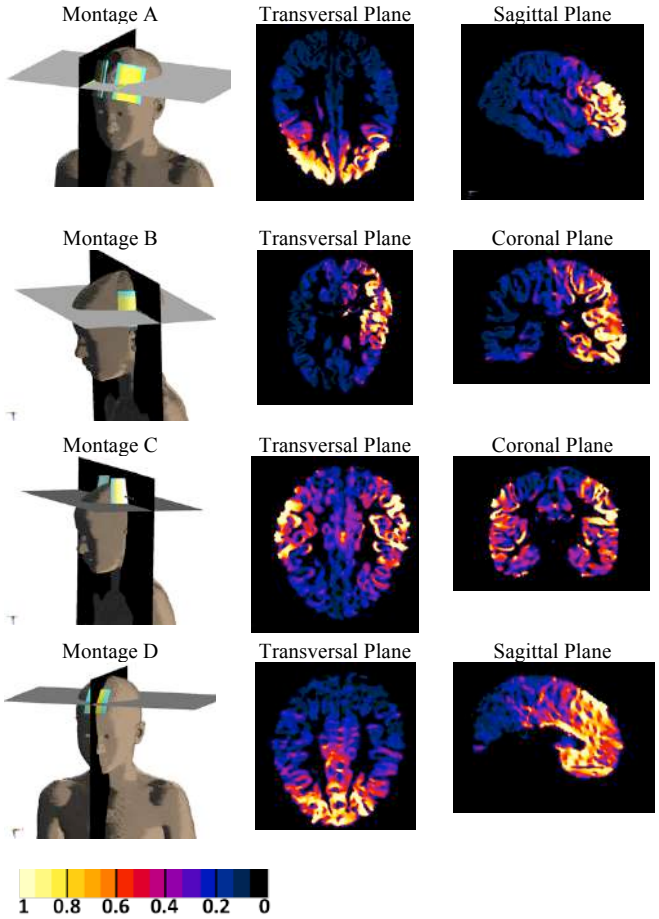

Fig. 1 Brain sections across the gray matter of the spatial distribution of the amplitude of **E**/**J** for "Billie" for all the four electrode montages. The other tissues and brain regions have been masked of the images.

for any human model, whereas the electrodes montage characterized by a more widespread spatial distribution of the amplitude is Montage C.

To quantify the variation due to the human variability on the field values, Table I reports the coefficient of variability among the models (CV, in dB) of both the peak and of the median values of **E** ($\mathbf{E}_{peak}$ and $\mathbf{E}_{median}$), in different brain regions for all the montages. The higher variability (up to almost 6 dB) was found for the Montage A, while for the Montages B-D the higher variability was about 3 dB (Montage D, thalamus, CV of E_{peak}). Only for the Montage A, the CV of E_{peak} is lower than the CV for E_{median}, with the exception on the pons. On the contrary, for all the other Montages B-D, the variability of the peak is always higher than the one of the median, with the exception of the pons for all the montages.

IV Conclusions

Results of this study showed that the general trend of the spatial distributions of the field amplitude remains similar among the different human models, varying the electrode montages. However, the physical dimension of the subject and his/her morphological and anatomical characteristics somehow influence the detailed field distributions such as the field values.

TABLE I

COEFFICIENT OF VARIABILITY (IN dB) OF THE PEAK AND OF THE MEDIAN OF **E** DUE TO THE VARIATION OF THE HUMAN MODEL IN DIFFERENT BRAIN TISSUES.

	CV of E_{peak} (dB)	CV of E_{median} (dB)
	Montage A	
Cortex	3.96	4.93
White	4.27	5.07
Cerebellum	5.47	5.70
Pons	5.54	5.08
Midbrain	5.04	5.38
Medulla	4.76	5.42
Thalamus	5.83	6.03
	Montage B	
Cortex	1.49	0.43
White	2.10	0.27
Cerebellum	1.97	0.94
Pons	1.52	1.79
Midbrain	1.82	1.06
Medulla	2.22	1.07
Thalamus	1.40	0.68
	Montage C	
Cortex	1.23	0.08
White	1.50	0.26
Cerebellum	0.75	0.37
Pons	1.14	1.70
Midbrain	2.19	1.10
Medulla	2.21	1.23
Thalamus	2.37	1.03
	Montage D	
Cortex	1.70	0.74
White	1.91	0.72
Cerebellum	0.93	0.67
Pons	1.05	1.39
Midbrain	2.16	0.87
Medulla	2.38	1.57
Thalamus	2.95	0.79

REFERENCES

[1] Brunoni AR, Nitsche MA, Bolognini N, et al. Clinical research with transcranial direct current stimulation (tDCS): Challenges and future directions. Brain Stimul 2011 Apr 1. [Epub ahead of print]

[2] M Bikson, A Rahman A, Datta F Fregni, L Merabet. High-resolution modeling assisted design of customized and individualized transcranial direct current stimulation protocols. Neuromodulation. 2012 Jul;15(4):306-15.

[3] M. Bikson, A. Rahman, A Datta, Computational Models of Transcranial Direct Current Stimulation *Clin EEG Neurosci, July 2012; vol. 43, 3: pp. 176-183*

[4] Christ A, Kainz W, Hahn GE, et al. The Virtual Family-development of surface-based anatomical models of two adults and two children for dosimetric simulations. Phys Med Biol 2010; 55: N23-N38.

[5] Gabriel S, Lau RW, Gabriel C. The dielectric properties of biological tissues: II. Measurements in the frequency range 10 Hz to 20 GHz. Phys Med Biol 1996; 41:2251-2269.

[6] Gabriel C. Comments on Dielectric properties of the skin. Phys. Med. Biol. 1997; 42: 1671-1674.

[7] B. Dell'osso, S. Zanoni, R. Ferrucci, et al., "Transcranial direct current stimulation for the outpatient treatment of poor-responder depressed patients," Eur Psychiatry, 2011 [Epub ahead of print]

[8] M. Macis, F. Mameli, M. Fumagalli, et al., "On-line Transcranial Direct Current Stimulation (TDCS) in aphasia," Neurol Sci; vol.31, pp. S37, 2010.

[9] F. Cogiamanian, S. Marceglia, G. Ardolino, S. Barbieri, A. Priori, "Improved isometric force endurance after transcranial direct current stimulation over the human motor cortical areas," Eur J Neurosci;vol 26(1), pp. 242-249, 2007.

[10] Y, Vandermeeren J Jamart and M Ossemann 2010 Effect of tDCS with an extracephalic reference electrode on cardio-respiratory and autonomic functions BMC Neurosci. 11 38.